JAMES | Journal of Advances in Modeling Earth Systems

RESEARCH ARTICLE
10.1029/2019MS001647

Special Section:
Community Earth System Model version 2 (CESM2) Special Collection

Evolution of the Double-ITCZ Bias Through CESM2 Development

M. D. Woelfle[1,2], C. S. Bretherton[1,3], C. Hannay[4], and R. Neale[4]

[1]Department of Atmospheric Sciences, University of Washington, Seattle, WA, USA, [2]Jupiter Intelligence, Inc., San Mateo, CA, USA, [3]Department of Applied Mathematics, University of Washington, Seattle, WA, USA, [4]National Center for Atmospheric Research, Boulder, CO, USA

Key Points:
- Increased southeast Pacific cloud fraction and improved SST gradients alleviate the double-ITCZ bias in CESM2
- Increased cloud fraction is driven by retuning of liquid cloud microphysics not the implementation of CLUBB boundary layer scheme
- Despite improvements in east Pacific precipitation, the global mean ITCZ position and cold tongue biases show no consistent change

Supporting Information:
- Supporting Information S1

Correspondence to:
M. D. Woelfle,
woelfle@uw.edu

Citation:
Woelfle, M. D., Bretherton, C. S., Hannay, C., & Neale, R. (2019). Evolution of the double-ITCZ bias through CESM2 development. *Journal of Advances in Modeling Earth Systems*, *11*, 1873–1893. https://doi.org/10.1029/2019MS001647

Received 5 FEB 2019
Accepted 14 MAY 2019
Accepted article online 20 MAY 2019
Published online 1 JUL 2019

Abstract The structure of the east Pacific Intertropical Convergence Zone (ITCZ) as simulated in the Community Earth System Model version 2 (CESM2) is greatly improved as compared to its previous version, CESM version 1. Examination of intermediate model versions created as part of the development process for CESM2 shows the improvement in the ITCZ is well correlated with a reduction in the relative warmth of southeast Pacific sea surface temperatures (SSTs) as compared to the broader tropical mean. Cooling SST in this region enhances the zonal SST and surface pressure gradients and reduces the anomalously southward SST gradient present in boreal spring in early version of CESM2. The improvements in southeast Pacific SST are attributed to increases in low cloud cover and the associated shortwave cloud forcing over the southeast. Sensitivity tests using fixed SST simulations demonstrate the increase in cloud cover between two intermediate model versions, 119 and 125, to be driven by removal of the dependence of autoconversion and accretion rates on cloud water variance as well as the removal of a secondary condensation scheme. Both of these changes reduce drizzle rates in warm clouds increasing cloud lifetime and cloud fraction in the stratocumulus to trade cumulus transition region. The improvements in southeast Pacific shortwave cloud forcing and ITCZ climatology persist through subsequent changes to the cloud microphysics parameterizations. Despite improvements in the east Pacific ITCZ, the global mean ITCZ position and Pacific cold tongue bias strength do not exhibit a systematic improvement across the development simulations.

1. Introduction

Accurate simulation of precipitation and sea surface temperatures (SSTs) in the deep tropics requires accurate representation of surface energy and momentum exchanges, atmospheric and oceanic circulations, and numerous parameterized processes including clouds and radiation. As a result of this complexity, proper simulation of these fields by coupled global climate models (GCMs) has remained an elusive goal for decades.

In observations, annual mean precipitation across the tropical Pacific basin is concentrated into two major features: the Intertropical Convergence Zone (ITCZ) and the South Pacific Convergence Zone (SPCZ). The ITCZ appears as an unbroken, zonal band of precipitation centered near 7°N in the annual mean (Hubert et al., 1969; Mitchell & Wallace, 1992; Waliser & Gautier, 1993; Zhang, 2001). The ITCZ shifts meridionally on seasonal time scales, as it is coupled with the seasonally migrating Hadley circulation. In the east Pacific, this seasonal migration manifests as a single, northern hemispheric maximum in precipitation from May through February. In the remaining months, a weak southern hemispheric ITCZ develops in the central and eastern Pacific, mirroring its northern counterpart.

Unlike the ITCZ, the SPCZ exists in the southwestern tropical Pacific year-round. Rain rates in the SPCZ are comparable to the northern hemispheric ITCZ and more intense than the seasonally appearing southern hemispheric ITCZ of the east Pacific. The SPCZ begins over the Maritime Continent and experiences a southeast tilt as it extends eastward into the central Pacific. As a result of this tilt, in the annual mean, there is a triangular-shaped dry region in the southeast Pacific basin bounded by the ITCZ to the north, the SPCZ to the south and west, and the South American coast to the east. This dry region in the southeast Pacific is dominated by trade cumulus and stratiform clouds and has proved difficult to accurately simulate in fully coupled GCMs (Lin, 2007; Li & Xie, 2014; Mechoso et al., 1995).

In most fully coupled GCMs, the ITCZ migrates into the southern hemisphere too early and remains too long. Thus, the annual mean, zonal mean precipitation field exhibits two maxima, one in each hemisphere, while only a single pronounced maxima is seen in observations (Lin, 2007; Li & Xie, 2014; Mechoso et al., 1995). The canonical label for this precipitation bias, the double-ITCZ bias, is derived from this profile. While the bias characteristics have improved slightly with increased model resolution and updated physics, the double-ITCZ bias persists in most GCMs participating in the Coupled Model Intercomparison Project, version 5 (Li & Xie, 2014; Taylor et al., 2012). While the double-ITCZ bias is often described using global, zonal means, it is particularly apparent in the east Pacific where the overly strong southern ITCZ protrudes into the observed dry southeast region.

Early efforts to understand and ameliorate the double-ITCZ bias focused on the role of low clouds in the southeast Pacific. Increasing low cloud cover in this region, whether through prescribed increases or through nonphysical parameterization changes, yielded improvements in the structure of the annual mean east Pacific ITCZ (de Szoeke et al., 2006; Ma et al., 1996; Yu & Mechoso, 1999). However, the improvements in the climatological precipitation field were often accompanied by a reduction in equatorial Pacific SSTs, that is, an amplification of the so-called cold tongue bias.

The inverse sensitivities of the double-ITCZ and cold tongue biases to southeast Pacific low cloud fraction prompted investigation into other local processes, particularly the role of excessive convective activity and its relationship with local SSTs (e.g., Hirota et al., 2011; Oueslati & Bellon, 2015; Song & Zhang, 2009; Wang et al., 2015). Biases in simulated convective activity can amplify via coupled feedbacks (Zhang et al., 2007; Liu et al., 2012). These feedbacks provide an explanation for why the double-ITCZ bias is stronger in fully coupled GCMs than in GCMs where SSTs are prescribed from observations (Lin, 2007; Li & Xie, 2014). Model simulations exploring the SST sensitivity show prescribing SST only over the southeast Pacific (from 5°S to 25°S and 120°W to the South American coast) is sufficient to ameliorate both the double-ITCZ and cold tongue biases in one otherwise fully coupled GCM (Song & Zhang, 2016). This result may be driven by local improvement or by improvements in the meridional gradient of SST which has been shown to be important in determining ITCZ structure in idealized experiments (Neale & Hoskins, 2000). Further sensitivity studies have suggested processes controlling boundary layer humidity are important for the ITCZ as moister boundary layers favor triggering of deep convection (Bacmeister et al., 2006; de Szoeke et al., 2006; Wang et al., 2015).

While local processes are important for determining the position and character of the east Pacific ITCZ, remote processes can also influence the position and strength of the Hadley Circulation and the embedded ITCZ (e.g., Kang et al., 2008; Lindzen & Hou, 1988). Slab ocean studies showed the zonal mean ITCZ position to be sensitive to a wide range of energetic forcings including ocean heat transport (e.g., Broccoli et al., 2006; Kang et al., 2018, 2014; Seo et al., 2014; Yoshimori & Broccoli, 2008), aerosol and cloud forcings (Yoshimori & Broccoli, 2008, 2009), and sea ice and land ice extent (Chiang et al., 2003; Chiang & Bitz, 2005; Mahajan et al., 2011). Modeling studies using fully coupled GCMs show a similar ITCZ response to those using a slab ocean when a forcing is applied to the northern Atlantic (Chiang et al., 2008; Dong & Sutton, 2002).

Based on this energetic framework, Hwang and Frierson (2013) proposed cloud forcing biases over the Southern Ocean may drive the double-ITCZ bias strength. However, a series of fully coupled model simulations suggests the fully coupled model response to cooling the southern high latitudes is dominated by anomalous oceanic rather than atmospheric energy transport (Kay et al., 2016; Hawcroft et al., 2016; Tomas et al., 2016). The differing response between the slab ocean and fully coupled experiments is in part due to the coupling of the near surface wind stress and upper ocean circulation in the tropics (Green & Marshall, 2017; Kang et al., 2018; Schneider, 2017) and reemphasized the importance of local forcings for driving the double-ITCZ bias.

Remarkably, the east Pacific double-ITCZ bias is greatly improved in the latest version of the National Center for Atmospheric Research's (NCAR's) fully coupled GCM, the Community Earth System Model version 2 (CESM2). This paper leverages a series of intermediate model versions created as part of the development process for this model to better understand both the double-ITCZ bias's sensitivities and the reasons for its improved tropical climatology. Section 2 describes the model versions, simulations, and data sets used in this study. Section 3 describes the improvements seen in CESM2 and the mechanisms behind the improvement. Finally, we summarize the results and discuss implications for future modeling efforts in section 4.

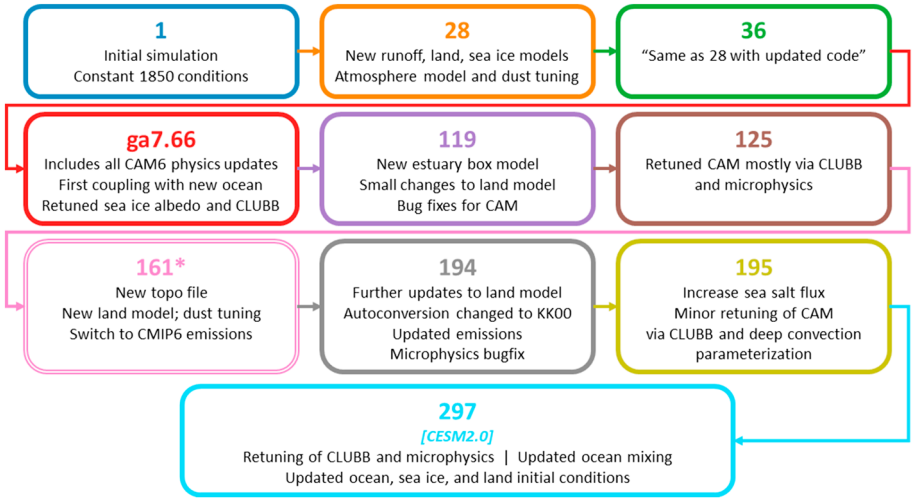

Figure 1. Model versions considered in this study. Details in each box described the major differences between a given version and its predecessor. All model simulations are historical simulations except for 161 as indicated by the asterisk. This simulation is a transient historical simulation. Further details are available in Text S1. CAM = Community Atmosphere Model; CLUBB = Cloud Layers Unified By Binormals; CESM = Community Earth System Model; CMIP = Coupled Model Intercomparison Project.

2. Methods

2.1. Model Versions Examined

This study examines the evolution of the double-ITCZ and cold tongue biases through the development of CESM2. To better understand the sensitivities and drivers of these biases, intermediate model versions created as part of the development process are examined alongside two released versions of CESM. All versions of CESM examined in this study consist of active atmosphere (Community Atmosphere Model [CAM]), land (Community Land Model), and river routing models. The fully coupled CESM system also includes prognostic ocean (Parallel Ocean Program version 2) and sea ice (Community Sea Ice Model) components.

The process of developing CESM2 yielded hundreds of intermediate model versions. Bogenschutz et al. (2018) examined three of these versions spanning the transition from CAM5.3 to CAM5.5. Their study briefly mentioned an improvement in the ITCZ bias and attributed it to local rather than remote processes. Here we expand upon this investigation of intermediate model versions by performing a targeted investigation of the ITCZ and cold tongue bias evolutions across the model development process from the first coupling of the new model components, denoted as intermediate version 01, or simply 01, to the released CESM version 2.0 which corresponds to intermediate version 297. The specific subset of simulations examined in this study captures a number of significant model changes that occurred during the development process including changes to cloud physics, the addition of an estuary box model (Sun et al., 2017), and increased ocean atmosphere coupling frequency. A brief description of the model version progression is shown in Figure 1, while a more thorough description can be found in supporting information Text S1.

For reasons to be discussed in the following section, this study centers around intermediate versions 119 and 125. Both of these model versions use an early version of CAM6 as the atmospheric component. The two model versions feature identical land, ocean, runoff, and sea ice components. The CAM6 configurations of the two model simulation differ in three major ways.

First, 119 considers spatial cloud water variance when calling the Seifert and Beheng (2001) autoconversion and accretion schemes. This dependency is removed in 125. Removing the dependency on local cloud water variance is equivalent to assuming the cloud water is uniformly distributed rather than the more physically plausible assumption of having regions of elevated and depleted cloud water within the cloud field. As autoconversion and accretion rates are nonlinear functions of liquid water content ramping up with higher values of liquid water content, removal of the cloud water variance leads to an overall reduction in both of these process rates.

The second distinction between the atmospheric components of 119 and 125 is the toggling of the `clubb_do_liqsupersat` flag. In tests performed by NCAR, it was shown that the climate sensitivity of 119 was outside the range required to acceptably reproduce the observed twentieth century temperature increases. This sensitivity was attributed to a supersaturation adjustment added between the cloud macrophysics and the cloud microphysics parameterizations which exerted a strong control on cloud feedbacks. When active, this adjustment condenses all supersaturated water vapor present in the output from the cloud macrophysics scheme onto existing liquid cloud droplets prior to passing the model state to the cloud microphysics scheme. If there are no preexisting cloud droplets, new 6-μm-diameter droplets are nucleated with no consideration of the availability of cloud condensation nuclei. Thus, the liquid supersaturation adjustment serves as a simplified secondary condensation parameterization. This adjustment is active in 119 and disabled in 125.

Finally, four parameters in the atmosphere model were retuned between 119 and 125. Two of these parameters, `clubb_gamma_coeff` and `clubb_c14`, are part of the joint cloud macrophysics-shallow cumulus parameterization of CAM6: the Cloud Layers Unified By Binormals (CLUBB) scheme (Golaz et al., 2002b, 2002a). This parameterization predicts properties of dry turbulence as well as cloud properties for both stratiform and shallow convective clouds using a joint probability distribution of liquid water potential temperature, total water mixing ratio, and vertical velocity. These variables along with several of their first- and second-order moments are predicted using turbulent kinetic energy-based prognostic equations. Once determined, the moments are used to construct a probability density function for each of the prognosed variables. These probability density functions are subsequently used to determine the properties of the parameterized cloud field.

The first retuned CLUBB parameter, `clubb_gamma_coeff` or γ, controls the skewness of vertical velocity with larger values of γ producing larger skewness. Larger vertical velocity skewness is indicative of a less well-mixed boundary layer with more distinct updraft and downdraft regions. Guo et al. (2015) showed γ to be one of the strongest controls on low cloud fraction in CLUBB with larger values of γ, that is, greater vertical velocity skewness, yielding smaller low cloud fraction, particularly over oceanic regions. The second retuned CLUBB parameter, `clubb_c14` or C14, determines the Newtonian damping rate of horizontal velocity variance. Based on the sensitivities described in Guo et al. (2015), the effects of retuning C14 are expected to be secondary to the changes driven by the altered γ parameter and thus are not considered explicitly in this study. In 119, γ is set to 0.29 and C14 to 1.83. In 125, these values become 0.32 and 2.2, respectively.

The final two retuned parameters, `micro_mg_berg_eff_factor` and `micro_mg_dcs`, are part of the two-moment Morrison-Gettelman microphysics parameterization version 2 employed by CAM6 (Gettelman & Morrison, 2014). The first of these parameters, `micro_mg_berg_eff_factor` or the Bergeron efficiency factor, controls the rate at which cloud water is converted to cloud ice via the Bergeron-Findeisen process. Larger values of the Bergeron efficiency factor lead to a more rapid conversion from liquid to ice and thus a more rapid depletion of cloud liquid and buildup of cloud ice. The second microphysics parameter, `micro_mg_dcs` or DCS, is the diameter to which a cloud ice particle must grow before it is converted to snow and subsequently precipitated out of the cloud at a particular model level. Use of a larger DCS value enables the retention of larger ice particles within glaciated clouds. As both of these parameters are related to processes involving cloud ice, neither parameter directly affects liquid-only clouds. In 119, the Bergeron efficiency is set to 0.3, and DCS is set to 4.4×10^{-4} m. In 125, these values are 0.7 and 5.4×10^{-4} m, respectively.

A summary of the differences between the atmospheric components of 119 and 125 is provided in Table 1. Parameter settings for a number of sensitivity simulations are also included for reference.

2.2. Simulations

All model simulations presented in this study are performed using the finite volume dynamical core with a horizontal resolution of 0.9° latitude by 1.25° longitude for the atmosphere and land models. The atmosphere model has 32 vertical levels. The ocean and sea ice models are run on a nominally 1° grid with the northern hemisphere pole shifted to lie over Greenland.

Unless otherwise noted, the output of the fully coupled model simulations presented in this study consists of climatology files computed at various points in the model development process. Due to storage limitations, only atmospheric output files are available for these simulations. Furthermore, given that these simulations

Table 1
Values of Atmospheric Model Parameters Used for Simulations

Parameter/process	119/119f	125/125f	119f_gamma	119f_microp	119f_ice	119f_nocwv	119f_liqss
`clubb_do_liqsupersat`	True	*False*	True	True	True	True	*False*
`clubb_gamma_coeff`	0.29	*0.32*	*0.32*	0.29	0.29	0.29	0.29
`clubb_c14`	1.83	*2.2*	1.83	1.83	1.83	1.83	1.83
`micro_mg_berg_eff_factor`	0.3	*0.7*	0.3	*0.7*	*0.7*	0.3	0.3
`micro_mg_dcs`	4.4×10^{-4}	5.4×10^{-4}	4.4×10^{-4}	5.4×10^{-4}	5.4×10^{-4}	4.4×10^{-4}	4.4×10^{-4}
$\overline{q'^2_{cld}}$ in microphysics	True	*False*	True	*False*	True	*False*	True

Note. A lowercase f following the model version number indicates simulations run using prescribed sea surface temperatures. Italics indicate values changed from the values used in 119/119f.

were performed with the goal of model development rather than being specifically designed for sensitivity investigations, the fully coupled climatologies have inconsistent spin-up periods and averaging periods as shown in Table 2. Excluding 161, all fully coupled model simulations are run using preindustrial boundary conditions, for example, emissions and land surface phenology, representative of constant 1,850 conditions. Model version 161 is a transient simulation run from 1850 to present day.

In addition to the fully coupled simulations, a series of sensitivity simulations is performed to better understand the changes made between model versions 119 and 125. These model versions are selected for further investigation as their ITCZ structures differ greatly (section 3.1), but their construction is quite similar. The parameters listed in Table 1 are the only changes made to the model between versions 119 and 125. Due to technical constraints, these simulations were run using SSTs and sea ice cover prescribed from a present-day climatology of the HadISST data set (Rayner et al., 2003), thus complicating direct comparison with their fully coupled counterparts. As the SSTs are prescribed from a climatology, there is no variability in the forcing beyond the annual cycle. Because of this, there is no representation of ENSO in the fixed SST simulations. All forcing files used in the model including trace gas and aerosol emissions are prescribed from a similar present-day climatology. To distinguish the fixed SST simulations from the fully coupled simulations, an f is included at the end of the model version number for the fixed SST simulations, for example, 119 versus 119f.

The first two of the fixed SST sensitivity simulations used in this study, 119f and 125f, employ model configurations identical to their fully coupled counterparts save for the change from preindustrial to present-day forcings and the change from a dynamic ocean and sea ice models to prescribed values for these model components. Five additional simulations are performed to test the sensitivity of the modeling system to the tuning changes made between 119 and 125. In the first sensitivity test, 119f_gamma, all parameters are identical to their 119 values except for γ which is set to the value used in 125. The second sensitivity test, 119f_microp, examines the effect of the microphysics changes by setting both the Bergeron efficiency parameter and the autoconversion threshold, DCS, to their 125 values as well as disabling the

Table 2
Averaging Period and Boundary Forcing Era for Fully Coupled Model Versions Examined in This Study

Version	Years averaged	Era
01	15–34	1850
28	75–99	1850
36	21–40	1850
ga7.66	2–20	1850
119	2–9	1850
125	70–89	1850
161	1980–1999	Historical
194	100–119	1850
195	122–141	1850
297	131–139	1850

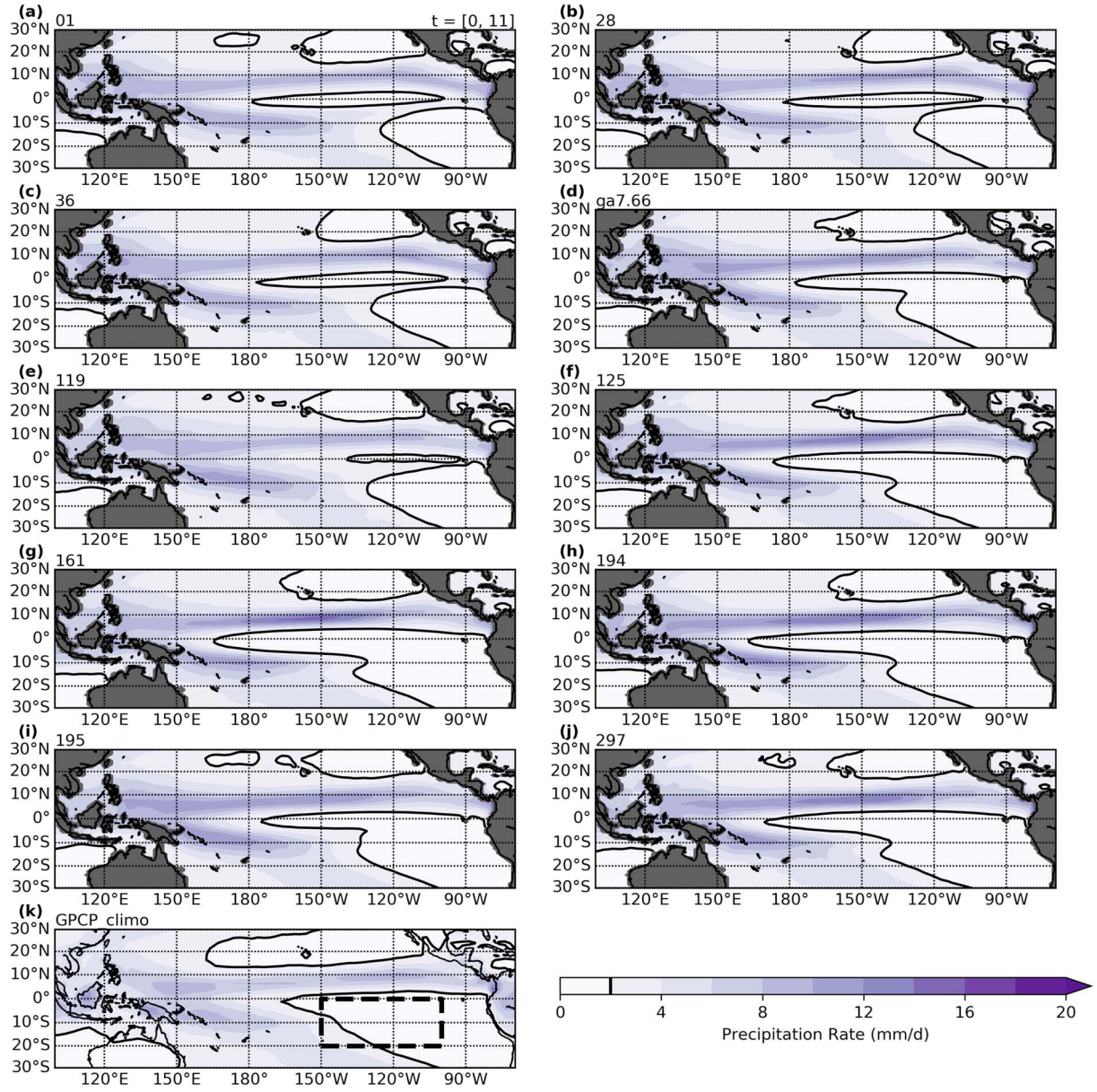

Figure 2. Annual mean precipitation rate for model versions (a) 01, (b) 28, (c) 36, (d) ga7.66, (e) 119, (f) 125, (g) 161, (h) 194, (i) 195, and (j) 297 as well as (k) for GPCP. The 2 mm/day precipitation rate contour is plotted as a solid black line. The region used to compute the double-Intertropical Convergence Zone index is outlined in (k) by the dashed black line. GPCP = Global Precipitation Climatology Project.

dependency of autoconversion and accretion rates on the cloud water variance. To further understand the microphysics sensitivities, two simulations are performed that separately examine the effect of either only changing parameters related to ice processes, 119f_ice, or only the assumption around cloud water variance, 119f_nocwv. The final sensitivity test, 119f_liqss, is identical to 119f save for disabling of the liquid supersaturation adjustment. The specific values of each parameter used in the fixed SST simulations are presented in Table 1. All fixed SST simulations are run for 10 years with years 2–10 taken for analysis.

All simulations presented in this study were run with interactive carbon and nitrogen cycles. Given the short spin-up period for these simulations, the carbon and nitrogen pools have likely not reached their final equilibrium states. However, impacts on the atmosphere are limited as atmospheric carbon dioxide concentrations are prescribed directly in these simulations. A fixed SST simulation in which plant phenology is prescribed from satellite observations showed the effect of carbon imbalances to have limited effect on the ITCZ as compared to the other model changes considered in this study. The effects of potential carbon

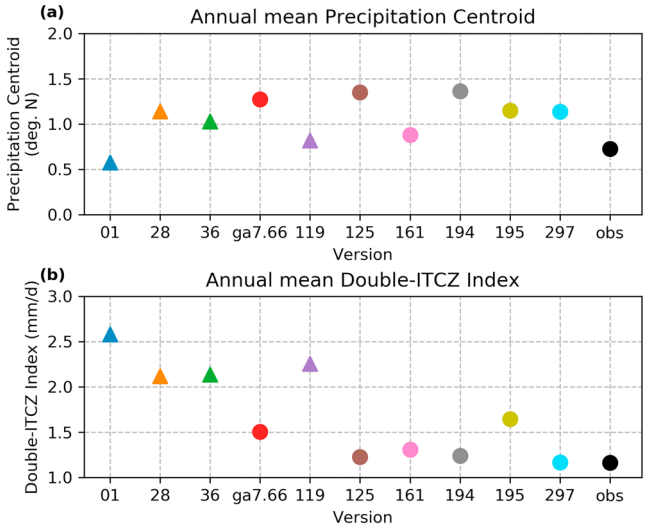

Figure 3. (a) Tropical precipitation centroid and (b) double-ITCZ index as a function of model version. Observed values computed from Global Precipitation Climatology Project are included in each panel for reference. Model versions with an annual mean double-ITCZ index greater than 2 mm/day are plotted with triangles. Model versions below this threshold are plotted with circles. ITCZ = Intertropical Convergence Zone.

pool imbalances in the fully coupled simulations are also expected to be secondary, but it is impossible to be certain as many of the development simulations cannot be repeated or extended due to changes to computing infrastructure at NCAR. Finally, initial condition files for CESM2 in which carbon pools are fully equilibrated were unavailable at the time of this study.

Simulations examined in this study were performed on the Yellowstone and Cheyenne (Computational And Information Systems Laboratory, 2017) supercomputing clusters. Simulation output is archived as Woelfle et al. (2019).

2.3. Comparison Data Sets

Observed precipitation fields are taken from the Global Precipitation Climatology Project (GPCP) version 2.1 (Huffman et al., 2009) for the period 1979–2009. Observed SSTs are taken from the same HadISST data set whose climatology is used to force the fixed SST simulations. Shortwave cloud forcing (SWCF) is taken from years 2000–2013 of the CERES-EBAF version 2.8 data set (Loeb et al., 2009). Surface pressure is taken from years 1979–2009 of the European Center for Medium Weather Forecasting's ERA-Interim reanalysis (Dee et al., 2011).

3. Results and Discussion

3.1. Model Bias Across Development Simulations

Prior to version ga7.66, CESM exhibits a canonical double-ITCZ precipitation structure in the Pacific basin (Figure 2). The bias is most recognizable in the southeast Pacific where modeled annual mean rain rates exceed 2 mm/day despite observed precipitation rates closer to 1 mm/day in this region. In version ga7.66, the first intermediate version using CAM6, the double-ITCZ bias is greatly improved (Figure 2d). However, the bias redevelops in 119 before returning to its improved state in all subsequent model versions. Full tropical mean precipitation rates are provided in Figures S1 and S2.

Despite the local improvement seen in annual mean southeast Pacific precipitation, global metrics for the double-ITCZ bias do not show consistent improvement. One such global metric is the tropical precipitation centroid:

$$\bar{C} = \frac{\int_{-20}^{20} [P(\phi)]\, \phi \, \mathrm{d}\phi}{\int_{-20}^{20} [P(\phi)]\, \mathrm{d}\phi}, \tag{1}$$

where $\bar{C}$ is the tropical precipitation centroid; P is the annual mean precipitation rate; ϕ is latitude; and $[\cdot]$ indicates zonal mean quantities. Positive values of the centroid are indicative of greater rainfall in the northern hemisphere tropics as compared to the southern hemisphere. The tropical precipitation centroid for CESM is generally biased northward as compared to observations, which is inconsistent with the excessive southern hemisphere rainfall characteristic of the double-ITCZ bias (Figure 3a). Furthermore, the tropical precipitation centroid shows little trend when plotted as a function of intermediate model version. This is at odds with the improvements seen in annual mean Pacific precipitation (Figure 2). Other global metrics for ITCZ position such as the precipitation assymmetry index of Hwang and Frierson (2013) show a similar lack of trend.

Alternatively, the Pacific double-ITCZ bias strength can be defined using a more local metric such as the mean precipitation rate over the southeast Pacific, 20°S to 0° and 100°W to 150°W (dashed black 2; Bellucci et al., 2010). For the remainder of this study, this local metric will be referred to as the double-ITCZ index. Unlike the global metrics, the double-ITCZ index well captures the improvements in modeled annual mean southeast Pacific precipitation (Figure 3b). The difference between the global and local bias metrics suggests the improvement in the east Pacific double-ITCZ bias seen in CESM2 is the result of local rather than remote processes as the latter must be mediated through global circulation changes.

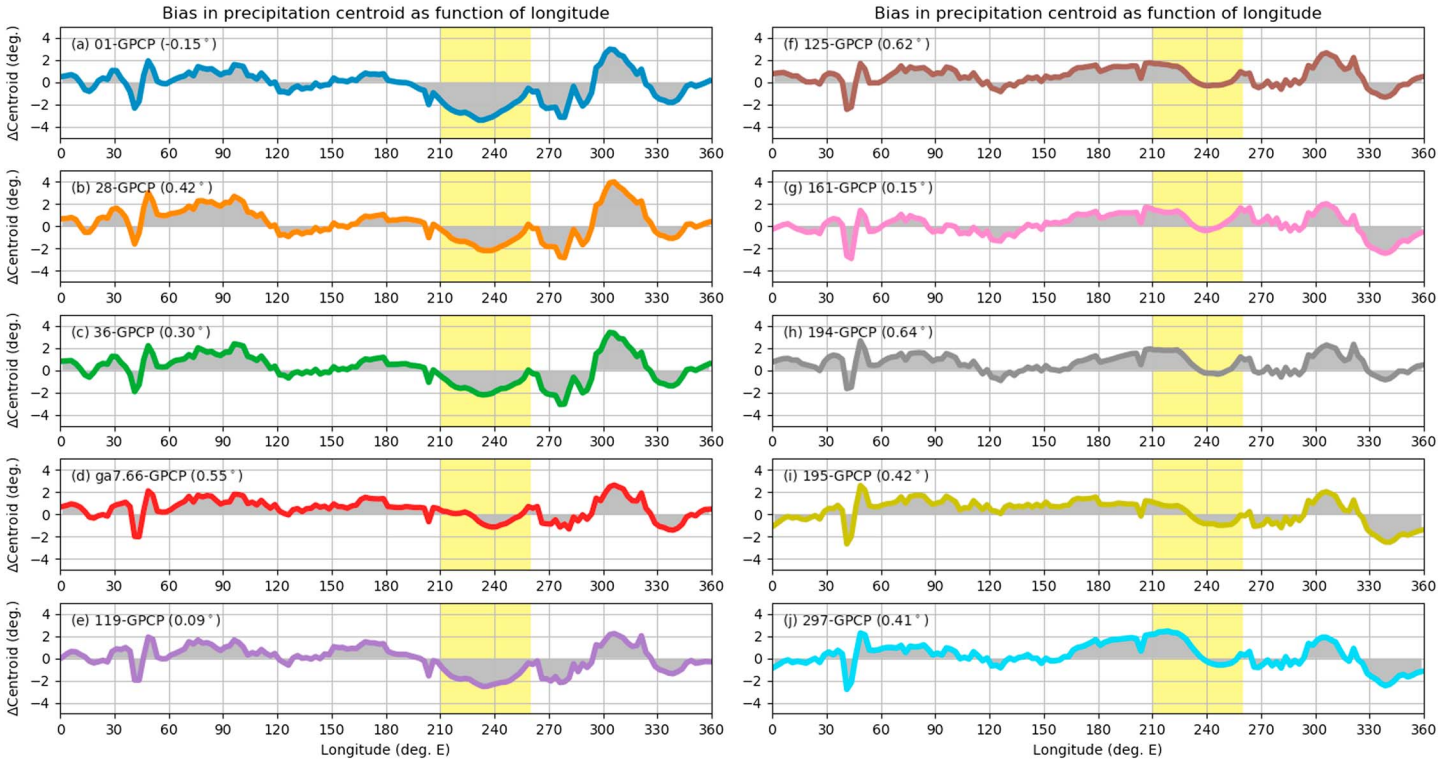

Figure 4. Precipitation centroid as a function of longitude differenced from the GPCP centroid for model versions (a) 01, (b) 28, (c) 36, (d) ga7.66, (e) 119, (f) 125, (g) 161, (h) 194, (i) 195, and (j) 297. The centroid of the zonal mean precipitation values are shown in parentheses. The longitude band used for computing the double-Intertropical Convergence Zone index is highlighted in yellow on each plot for reference. GPCP = Global Precipitation Climatology Project.

We can further assess the regional changes in tropical precipitation across model versions by examining the tropical precipitation centroid as a function of longitude rather than examining the centroid of the zonal mean profile. The latitude-weighted centroid is defined as

$$C(\theta) = \frac{\int_{-20}^{20} P(\theta, \phi)\phi \, \partial\phi}{\int_{-20}^{20} P(\theta, \phi) \, \partial\phi}, \tag{2}$$

where θ is longitude and all other variables are as defined in equation (1). Figure 4 shows the longitude-resolved centroid values for each model as a difference from the GPCP centroid values. The GPCP climatology is shown in Figure S3. The annual mean bias in east Pacific rainfall in model versions 01, 28, 36, and 119 is driven predominately by biases in boreal spring. These models also tend to have a northward bias in precipitation over the South American continent (300°E to 330°E) which maximizes in boreal fall. Both of these seasonal biases project strongly onto the annual mean. Improvements in the east Pacific rainfall bias are often accompanied by improvements over South America. Thus, annual mean, zonal mean metrics for the position of the ITCZ are unable to capture the improvements seen in the east Pacific. There also exists a large amplitude bias in precipitation centroid near 45°E which is associated with the inability of climate models to accurately model precipitation near the African coast. While Figure 4 reveals a number of biases in tropical precipitation, we focus here on the reduced east Pacific bias and leave characterization of other biases to future investigations.

The seasonal cycle of the double-ITCZ index is plotted in Figure 5a. While a small bias of approximately 1 mm/day exists in boreal summer and fall for all model versions, the amplitude of the annual mean bias is largely determined by the bias amplitude in late boreal winter and spring. The four model versions with the strongest double-ITCZ bias, 01, 28, 26, and 119, have southeast Pacific precipitation rates in excess of 4 mm/day in March and April, while observed precipitation from GPCP barely exceeds 2 mm/day. The boreal spring precipitation bias in ga7.66 and 195 is smaller at approximately 1 mm/day. Model versions 125, 161, 194, and 297 slightly underpredict boreal spring rainfall.

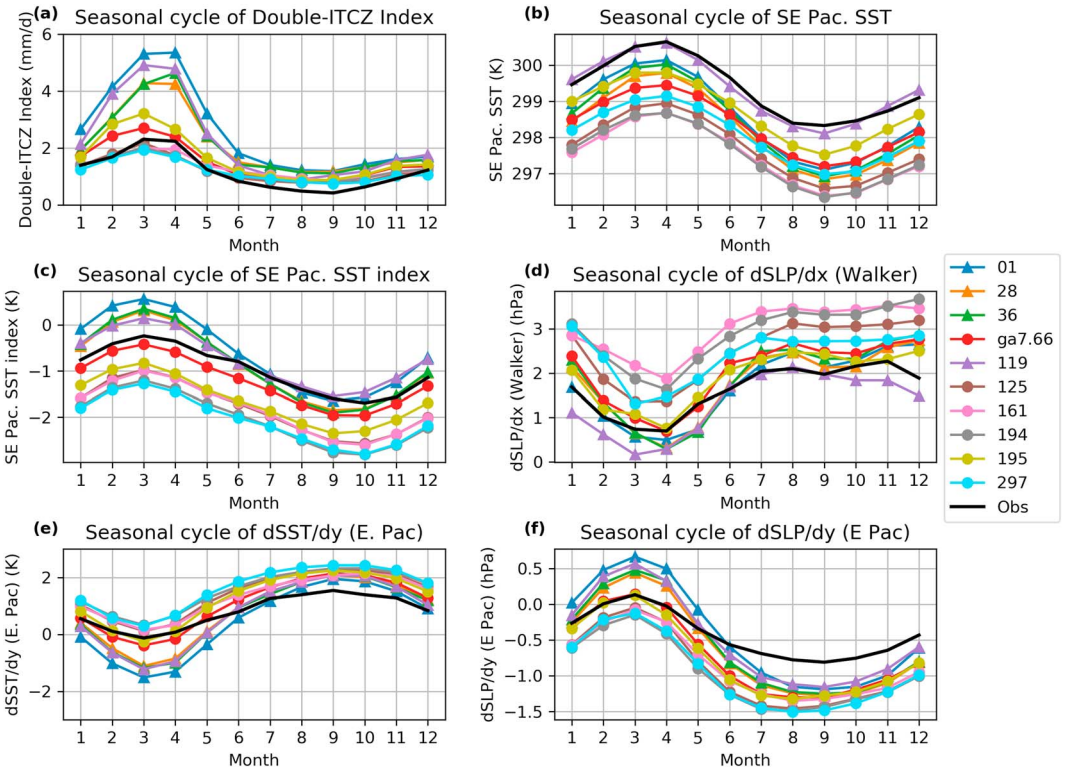

Figure 5. Seasonal cycle of (a) the double-ITCZ index, (b) southeast Pacific SST, (c) the southeast Pacific SST index, (d) the zonal surface pressure gradient, (e) the east Pacific meridional SST gradient, and (f) the east Pacific meridional surface pressure gradient for fully coupled simulations and observations. Model versions with an annual mean double-ITCZ index greater than 2 mm/day are plotted with triangles. Model versions below this threshold are plotted with circles. ITCZ = Intertropical Convergence Zone; SST = sea surface temperature.

Many previous studies of the double-ITCZ bias suggest the bias is associated with elevated SSTs in the southeast Pacific whether through locally anomalous surface heating or ocean advection (Liu et al., 2012; Oueslati & Bellon, 2015). Absolute SSTs over the southeast Pacific are unable to fully differentiate the simulations with poor ITCZs from those which more accurately simulate precipitation in the east Pacific (Figure 5b). In particular, the local precipitation rate in 28 is 1 mm/day greater than in 195 despite nearly identical underlying mean SST. Furthermore, a direct comparison of southeast Pacific SST across all of the coupled simulations is not straightforward as the majority of the simulations are run under preindustrial conditions when observations are limited, and one model version, 161, is run using present-day forcings. Additionally, model simulations were tuned for top-of-atmosphere energy balance which may result in differing relationships between local SST in the southeast Pacific and the global mean. Thus, we next examine the relative warmth of the southeast Pacific by defining a southeast Pacific SST index which is computed as the mean SST over the same region as the double-ITCZ index (20°S to 0° and 100°W to 150°W) minus the tropical mean SST (20°S and 20°N). In a 1979–2005 climatology of the HadISST data set, the southeast Pacific SST index is negative year-round reflecting the relatively cool SSTs in this region as compared to the tropical mean (Figure 5c). However, models with a strong double-ITCZ bias exhibit southeast Pacific SSTs that exceed the tropical mean in boreal spring.

Low-level circulations in the deep tropics are strongly controlled by the underlying SST gradient with low-level flow oriented along the surface temperature gradient toward higher SSTs (Lindzen & Nigam, 1987). Thus, it is unsurprising that the strength of the east Pacific double-ITCZ bias is well captured by the southeast Pacific SST index. Elevated SSTs in the southeast Pacific relative to the tropical mean decreases the climatological zonal and meridional temperature gradients in the tropical Pacific. The reduction in zonal temperature gradient weakens the Walker Circulation by reducing the zonal surface pressure gradient along the equator (Figure 5d). The zonal surface pressure gradient is computed here as the mean near-equatorial surface pressure of the east Pacific (5°S to 5°N and 80°W to 160°W) minus the mean near-equatorial sur-

face pressure of the west Pacific (5°S to 5°N and 80°W to 160°W; DiNezio et al., 2013). Computing the Walker Circulation strength using latitude limits of ±3° and ±10° latitude showed similar results. The weakened Walker Circulation decreases subsidence in the eastern Pacific, reducing one limitation on convective activity in the region.

The local increase in southeast Pacific SST also directly impacts the meridional SST gradient in the east Pacific (Figure 5e). We define the east Pacific meridional SST gradient as the difference between the mean near-equatorial SST in the northeast Pacific (0° to 10°N; 100°W to 150°W) and the mean near-equatorial SST of the southeast Pacific (10°S to 0°; 100°W to 150°W). Positive values indicate warmer temperatures in the northern hemisphere and, thus, imply southerly flow at the equator. For both observations and models with an improved double-ITCZ bias, the east Pacific meridional SST gradient is directed northward in all months except boreal spring when ga7.66, 195, and observations exhibit a weak southward gradient. The four model versions with strong double-ITCZ biases have a much stronger SST gradient reversal in the boreal spring which is indicative of northerly flow at the equator. This circulation is associated with enhanced southern hemispheric convergence and convection.

Interestingly, the northward-oriented meridional SST gradient is too strong in boreal fall in all model simulations. This may drive overly strong northern hemispheric precipitation during this period. As we are most interested in the southeast Pacific rainfall biases which maximize in boreal spring, the implications of the boreal fall SST bias are left for future investigations.

The meridional surface pressure gradient is dynamically consistent with the collocated SST gradient (Figure 5f). The relatively cool water of the southeast Pacific leads to a local high pressure, a southward oriented pressure gradient, and resultant southerly flow. The boreal spring pressure gradient is near zero in ERAI, biased northward in models with a strong double-ITCZ bias and either accurately modeled or biased southward in the simulations with an improved east Pacific ITCZ structure. This tight coupling of the southeast Pacific double-ITCZ bias and local SST and surface pressure gradients is consistent with the CESM1 bias characteristics described in Wang et al. (2015). Because the observed SST and surface pressure gradients in the east Pacific in boreal spring are near 0, there is little margin for error in simulating the dynamics of this region.

In this section, we have examined the amplitude of the southeast Pacific precipitation bias as a function of model version for a number of intermediate CESM development simulations leading toward CESM2. We have shown the differences in bias amplitude are unlikely to be driven by remote processes as global metrics of the ITCZ bias are inconsistent with local precipitation changes. Furthermore, we have shown the east Pacific double-ITCZ bias in these simulations is well correlated with the relative warmth of the southeast Pacific due to its projection onto zonal and meridional SST gradients. The effect of the meridional SST gradient is consistent with previous studies of the double-ITCZ bias. The results thus far constitute an internally consistent description of the east Pacific double-ITCZ bias but do not provide a mechanistic understanding of the drivers of the bias. In order to explore possible mechanisms for the double-ITCZ bias improvement in CESM2, we next undertake a closer examination of two intermediate model versions, 119 and 125, which, despite being quite similar in their construction, exhibit strikingly different ITCZ bias amplitudes.

3.2. Bias Sensitivity: The Difference Between 119 and 125

To better understand the driver(s) of the bias improvement from 119 to 125, we perform a series of sensitivity tests in which we isolate several of the changes made between these two versions. These sensitivity tests are performed using SSTs and sea ice prescribed from a present-day climatology as this is the only model configuration which could be run on the available computational infrastructure. Prescribing SST and sea ice from a present-day climatology allows assessment of the atmosphere model's ability to simulate the east Pacific ITCZ region independent of ocean feedbacks and biases. These simulations seek to isolate each of the changes made between 119 and 125 with emphasis on the changes to cloud parameters and parameterizations. 119f and 125f are the fixed SST counterparts of 119 and 125, respectively. The atmosphere component of these fixed SST simulations is identical to their fully coupled versions. The sensitivity tests isolate the effects of updating the vertical velocity skewness parameter (119f_gamma), modifying the liquid and ice cloud microphysics parameterizations (119f_microp), retuning only the ice microphysics (119f_ice), only removing the autoconversion and accretion dependence on cloud water variance (119f_nocwv), and disabling the liquid supersaturation adjustment (119f_liqss). Other than the listed modifications, each of these

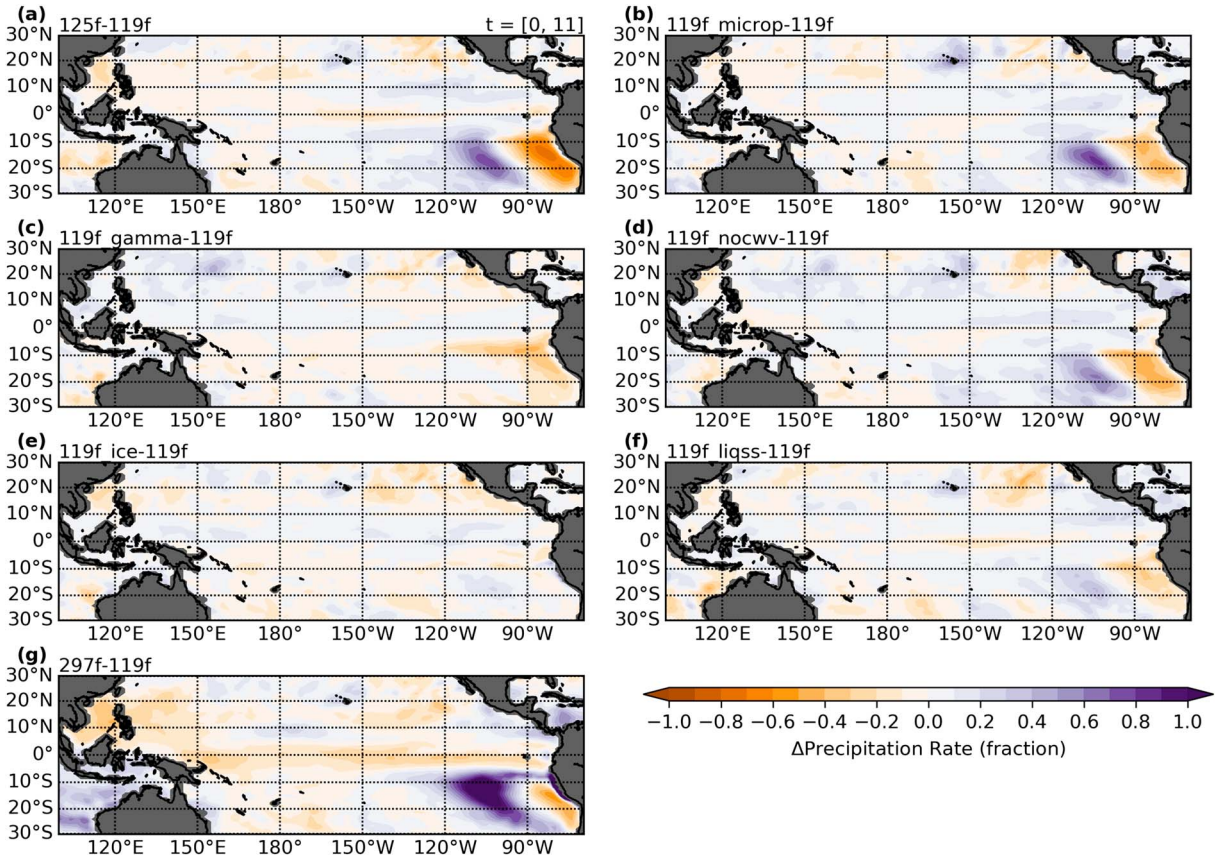

Figure 6. Fractional difference in annual mean precipitation rate from 119f for (a) 125f, (b) 119f_microp, (c) 119f_gamma, (d) 119f_nocwv, (e) 119f_ice, (f) 119f_liqss, and (g) 297f.

five model configurations are identical to 119f. Description of the model configuration for each sensitivity test is provided in Table 1, and further description of each modification is provided in section 2.2.

The differences in surface wind stress and absolute precipitation rate between 125f and 119f are small as these fields are tightly constrained by the prescribed SST field, especially for convective precipitation. Precipitation rates, on the other hand, show large relative changes between 119f and 125f in the southeast Pacific with a decrease in precipitation by up to 70% east of 90°W and a similar increase between 90°W and 120°W by up to 70% (Figure 6). The annual mean precipitation rate for 119f is shown in Figure S4.

The southeast Pacific precipitation dipole is well captured by the microphysics changes only simulation, 119f_microp, though the amplitude of the drying is slightly weaker (Figure 6). Comparison of the precipitation changes in 119f_nocwv and 119f_ice shows the precipitation response to be driven primarily by the change in dependency on cloud water variance rather than the changes to ice microphysics. Disabling of the liquid supersaturation adjustment in 119f_liqss produces a similarly signed precipitation response, though the magnitude is much weaker. Finally, increasing the CLUBB γ parameter leads to a decrease in southern hemispheric precipitation east of 90°W. A secondary region of reduction extends westward and along 10°S out to 120°W.

While surface wind stress and large-scale precipitation features are largely pinned in place by the prescribed SSTs, the low cloud field can more readily respond to changes in atmospheric parameterizations. The largest changes in Pacific low cloud fraction between 119f and 125f are found in the same region as the largest relative precipitation rate response, the southeast stratus and stratocumulus regions (Figure 7a). Figure 7a shows the difference in cloud fraction in contours over the 119f climatological cloud fraction in color. In the 119f climatology, cloud fraction is highest near the South American coast and decreases with increasing distance from shore. The region of decreasing cloud cover is known as the stratocumulus to trade cumulus transition region and is a difficult region for GCMs to properly simulate. Relative to 119f, 125f has decreased

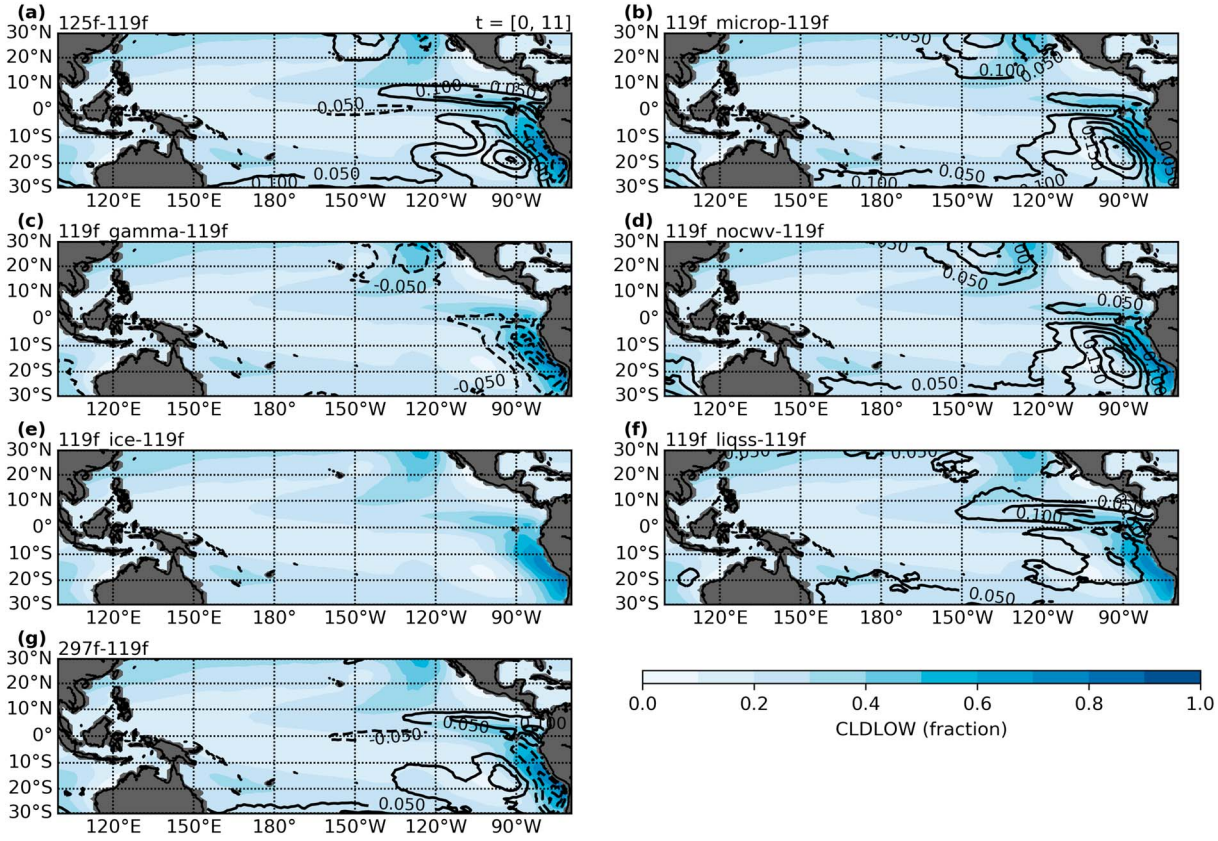

Figure 7. The difference in low cloud fraction from 119f is plotted in contours for (a) 125f, (b) 119f_microp, (c) 119f_gamma, (d) 119f_nocwv, (e) 119f_ice, (f) 119f_liqss, and (g) 297f. Positive contours are solid lines. Negative contours are dashed. The contour interval is 0.05. The zero contour is not plotted. The annual mean cloud fraction from 119f is plotted in color on each figure.

low cloud cover in the climatological stratus region near the South American coastline where cloud fraction is initially quite high. Conversely, low cloud fraction increases in the stratocumulus to trade cumulus transition region of 125f. This dipole in cloud response results from a superposition of the responses to the microphysics and CLUBB adjustments made between 119 and 125.

In 119f_microp, absolute low cloud fraction increases by up to 25% in the transition region with little change near the South American coastline (Figure 7b). As with the precipitation response, the response to microphysical changes in this region is driven by the change to the autoconversion and accretion schemes rather than the cloud ice parameters (Figures 7d and 7e). Removing the autoconversion and accretion dependence on cloud water variance is equivalent to assuming a homogeneous cloud with evenly distributed cloud water throughout. As the accretion and autoconversion rates are nonlinear with respect to cloud water, the effective smoothing of the cloud water field reduces the autoconversion and accretion rates in the model. This reduces the loss rate of cloud water to precipitation, enabling liquid clouds to both retain more cloud water and persist longer before dissipating. The relationship between reduced precipitation production and low cloud cover is evident in the 119f_nocwv model response. The maximum low cloud response in 119f_nocwv is located at 90°W, the saddle point in the fractional precipitation response dipole. To the east of this point, the altered microphysics lead to a reduction in precipitation prolonging the lifetime of the low cloud. The increased tendency of the model to maintain low cloud fraction leads to an extension of stratocumulus further off shore. Precipitation west of 90°W increases due to the change from generally nonprecipitating trade cumulus to precipitating stratocumulus clouds.

The low cloud response of 119f_liqss exhibits a similar southeast Pacific response to 119f_nocwv albeit of lesser magnitude. In 119f, the liquid supersaturation adjustment enhances the growth of cloud water droplets by condensing excess water vapor onto existing droplets. Removal of this parameterization slows the growth of liquid cloud droplets. This increases the cloud lifetime by delaying the loss of cloud water via pre-

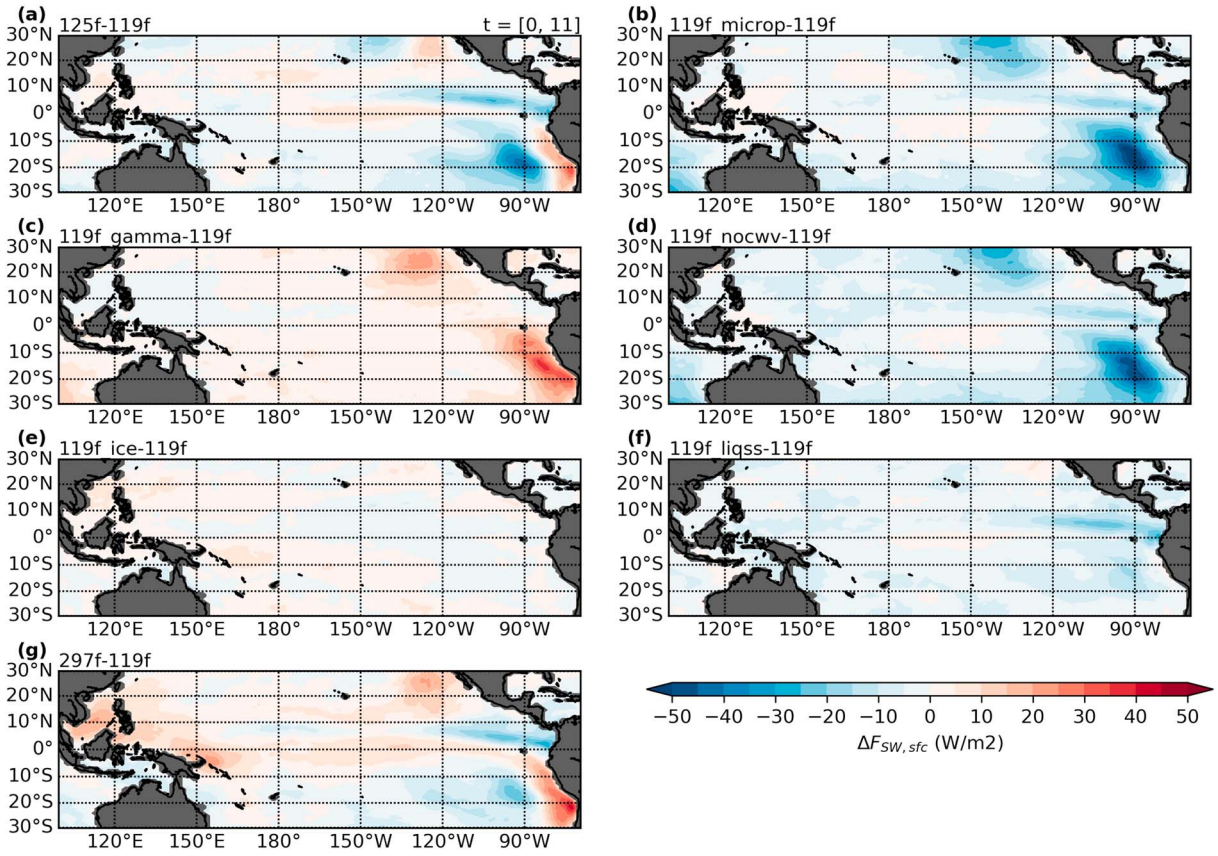

Figure 8. Annual mean net surface shortwave flux (a) 125f, (b) 119f_microp, (c) 119f_gamma, (d) 119f_nocwv, (e) 119f_ice, (f) 119f_liqss, and (g) 297f as a difference from 119f.

cipitation. This is similar to the effect seen in 119f_nocwv. 119f_liqss shows additional low cloud increases in the northern ITCZ region likely resulting from the large low-level moisture convergence in this region.

From 119f to 119f_gamma, the vertical velocity skewness parameter, γ, is increased from 0.29 to 0.32. As a result, the skewness of vertical velocity increases. Conceptually, this is equivalent to the boundary layer becoming less well mixed. The effect of this change is strongest in the stratus region, east of 90°W, where the increase in skewness drives a transition from continuous stratus decks to broken fields of stratocumulus (Figure 7c). Further offshore, where vertical velocities are generally already skewed positive and cloud field is already broken, the further increase in skewness has limited effect.

The cloud response dipole of 125f drives a similar response in the net surface shortwave flux (Figures 8a). The reduction in cloud cover near the South American coast allows the net surface shortwave radiative flux to increase by up to 25 W/m^2 in 125f as compared to 119f. The opposite is true of the transition region further offshore where cloud fraction increases and the net surface shortwave radiative flux decreases by as much as 35 W/m^2 in 125f as compared to 119f. The sensitivity tests which isolate the changes to cloud microphysics, 119f_microp, and the changes to CLUBB, 119f_gamma, exhibit stronger surface heating rate changes than 125f as the microphysical and CLUBB driven changes to cloud fraction damp the individual responses. Consistent with its cloud response, the effect of disabling the liquid supersaturation adjustment drives a weaker but still similarly signed response to 119f_microp in the southeast Pacific. Were the surface temperatures of 125f allowed to respond the surface heating anomalies, the southeast Pacific, east of 90°W, would cool considerably before either reduced turbulent surface fluxes, increased cooling via cloud-SST feedbacks, or oceanic adjustments could bring the system into a new equilibrium. The reduced local surface heating in 125f as compared to 119f is consistent with the cooler southeast Pacific SST index of 125 as compared to 119 (Figure 5b). Thus, the increase in low cloud fraction over the southeast Pacific in 125 as compared to 119 is likely responsible for its improved representation of the east Pacific ITCZ.

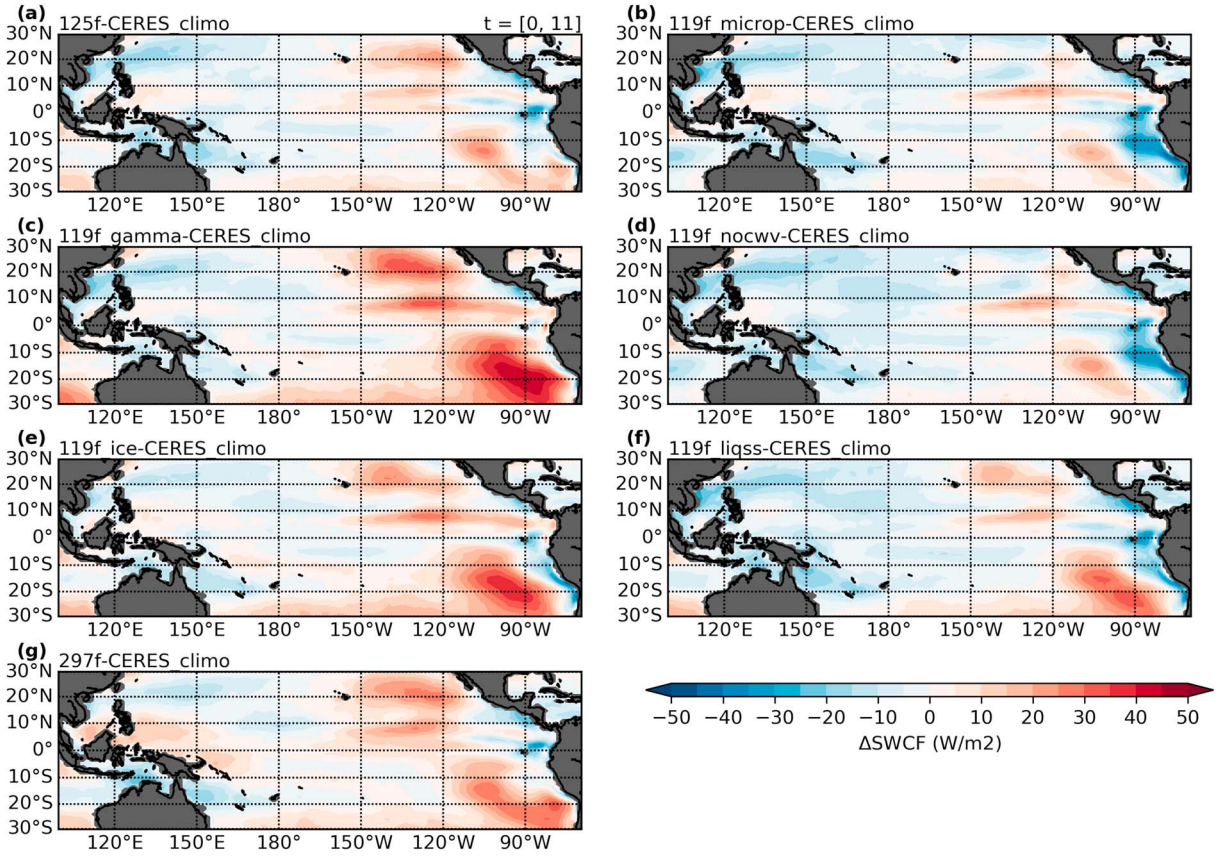

Figure 9. Annual mean shortwave cloud forcing for (a) 125f, (b) 119f_microp, (c) 119f_gamma, (d) 119f_nocwv, (e) 119f_ice, (f) 119f_liqss, (g) 297f, and (h) 119f as a difference from CERES. More negative values indicate more reflected insolation and a stronger SWCF. SWCF = shortwave cloud forcing.

The SWCF response in the fixed SST simulations is qualitatively indistinguishable from the surface shortwave flux response with increases (decreases) in SWCF in regions of increased (decreased) cloud cover. Thus, instead of examining the SWCF response with respect to 119f, Figure 9 shows the modeled SWCF for each of the fixed SST simulations as a difference from the 2000–2013 SWCF climatology of CERES-EBAF version 2.8 (Loeb et al., 2009). The reference CERES climatology is shown in Figure S5. For consistency with model output fields, SWCF is defined in this study as the difference between the net top-of-atmosphere shortwave flux when clouds are included in the model radiation calculation and the net clear sky shortwave flux. Negative values of SWCF indicate a shortwave cooling effect due to cloud cover.

The SWCF in the southeast Pacific of 119f is biased positive as compared to CERES. The bias maximizes near 90° W with an amplitude greater than 30 W/m^2. The increased cloud cover in the southeast Pacific of 125f is sufficient to reduce the SWCF bias to 10 W/m^2 over much of the southeast Pacific with only a small region exceeding 20 W/m^2, suggesting the improvements in the surface shortwave flux and its anticipated effect on the coupled ITCZ are driven by realistic improvements in the SWCF field. As in the previous discussion of surface fluxes and cloud fraction changes, the improvement from 119f to 125f is driven by changes to the cloud accretion and autoconversion parameterizations (Figure 9d) and opposed by the change to CLUBB's skewness parameter (Figure 9c). The removal of the liquid supersaturation adjustment drives a weak improvement in the SWCF, while the retuned ice microphysics have little to no effect.

3.3. Implications of the 119–125 Sensitivity Tests for CESM2

The differences in low cloud fraction (Figure 7a), surface shortwave flux (Figure 8a), and SWCF between 119f and 125f are qualitatively similar to the difference between a prescribed SST version of CESM2 (297f) and 119f (Figures 7g and 8g). Thus, the improved ITCZ structure in 297f as compared to 119f can also be attributed to the increase in low cloud cover over the southeast Pacific. The SWCF for the fully coupled simulations discussed in section 3.1 exhibits an increase in southeast Pacific SWCF from version 125 onward which is an amplified version of the response seen in the fixed SST simulation, 125f (Figure 10). The expected

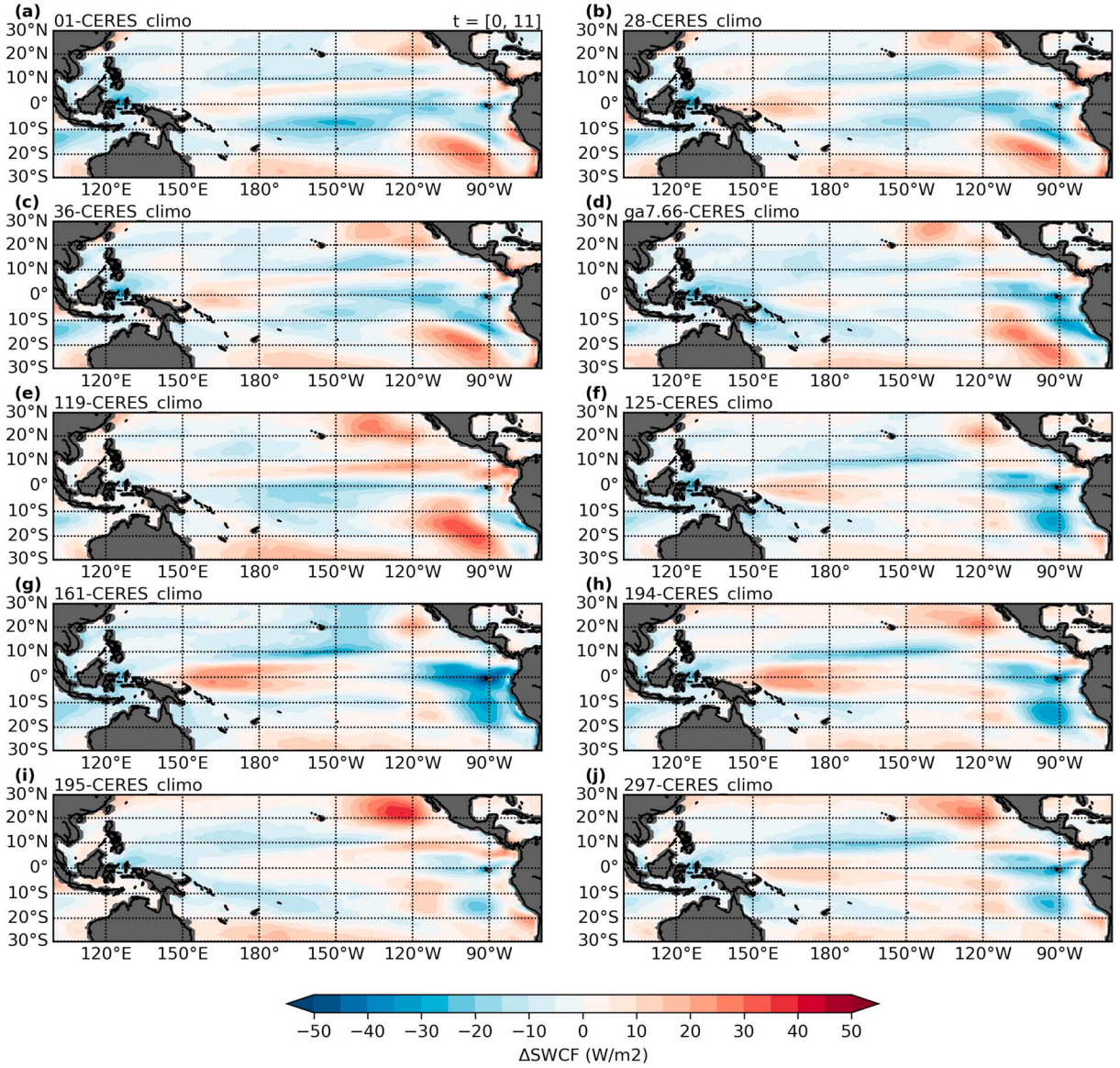

Figure 10. Annual mean shortwave cloud forcing for the fully coupled simulations (a) 01, (b) 28, (c) 36, (d) ga7.66, (e) 119, (f) 125, (g) 161, (h) 194, (i) 195, and (j) 297 as a difference from the 2000–2013 CERES climatology. More negative values indicate more reflected insolation and a stronger SWCF. SWCF = shortwave cloud forcing.

decrease in surface shortwave forcing is also present in runs with elevated SWCF and is consistent with the relatively cool SSTs over the southeast Pacific noted for simulations with an improved east Pacific ITCZ. Furthermore, the SWCF in simulations from version 125 onward has an elevated SWCF as compared to version 01 suggesting the increased cloud cover drives the overall improvement between version 01 and CESM2 as well.

In the sensitivity tests for the 119 and 125 model physics, the increased cloud cover in the southeast Pacific in 125 was attributed to the combined effects of disabling the liquid supersaturation adjustment and removing the dependency of autoconversion and accretion rates on cloud water variance. Together, these changes reduce precipitation in the stratus region thus increasing both cloud lifetime and the local SWCF. While the response in 297f is qualitatively similar to 125f, the mechanisms are somewhat different. Model version 125 uses the Seifert and Beheng (2001) scheme to compute the autoconversion and accretion rates, while 297 uses Khairoutdinov and Kogan (2000). Furthermore, the implementation of the autoconversion and

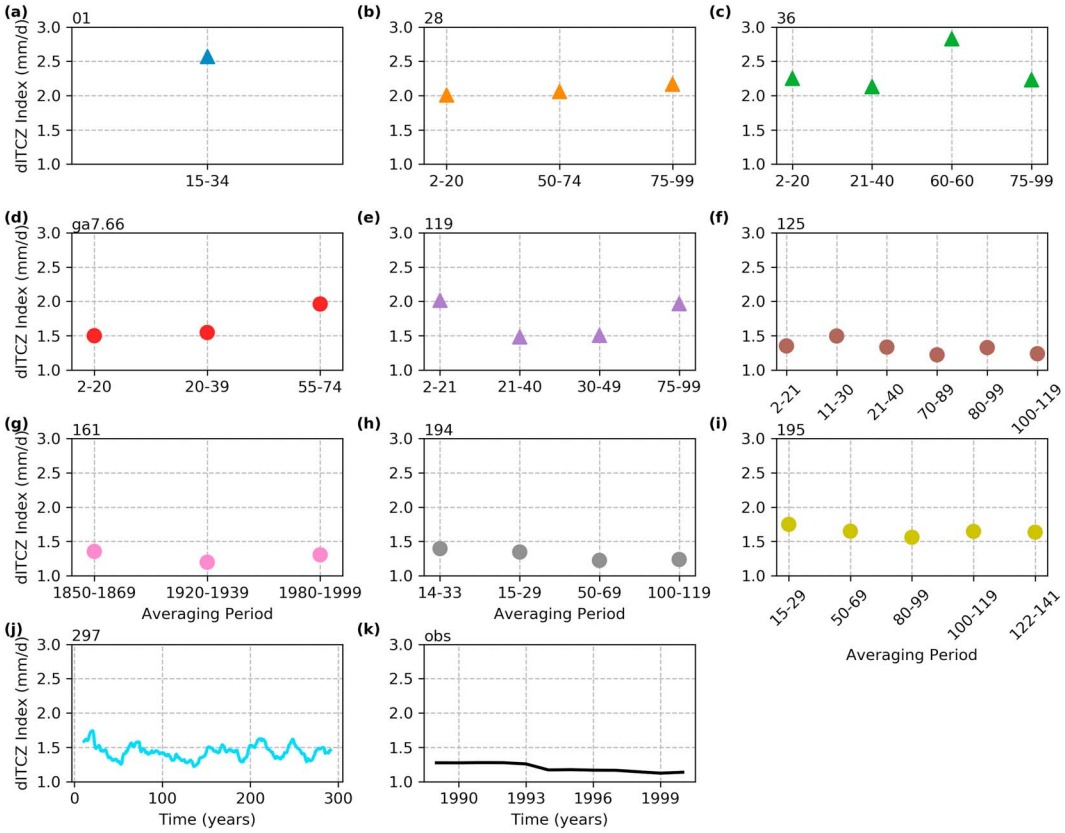

Figure 11. Annual mean double-ITCZ index as a function of averaging period from available climatologies for (a) 01, (b) 28, (c) 36, (d) ga7.66, (e) 119, (f) 125, (g) 161, (h) 194, and (i) 195. Twenty-year running means of the double-ITCZ index for (j) 297 and (k) Global Precipitation Climatology Project are also shown. Model versions with an annual mean double ITCZ index greater than 2 mm/day in the period listed in Table 2 are plotted with triangles. Model versions with a double-ITCZ index below this threshold are plotted using circles. ITCZ = Intertropical Convergence Zone.

accretion parameterization in 297 reinstates the effect of cloud water variance. Given this, there are several possible explanations for the continued SWCF improvement found in 297.

First, the SWCF improvement in 125f as compared to 119f was attributed to two model formulation changes: removal of the cloud water dependency and removal of the liquid supersaturation adjustment between cloud macrophysics and cloud microphysics. While the former is no longer true of 297, the liquid supersaturation is never reintroduced. It is possible the autoconversion and accretion process rates are similar between the Seifert and Beheng (2001) without considering cloud water variance and the Khairoutdinov and Kogan (2000) with this dependency. Regrettably, process rates are unavailable from the fully coupled model simulations. The qualitative similarity in the precipitation fields in the fixed SST simulations with drying near the coast and increased precipitation further offshore may support the argument of similar process rates, but the region of increase precipitation is much greater in 297 than 125 suggesting there may be other processes involved.

While the improved SWCF in the southeast Pacific can be invoked to explain the improved east Pacific rainfall climatology in version 125 through 297, it cannot explain the improved ITCZ in ga7.66 as the increased southeast Pacific SWCF is absent from this model version. In the averaging period considered throughout most of this study, ga7.66 has a similar SST structure as the other model versions with improved ITCZs (Figure 5), though the reasons for this improved climatology are somewhat unclear. In addition to the fully coupled climatologies listed in Table 2, climatologies for several other averaging periods are available. Examination of these other averaging periods shows the strength of the double-ITCZ bias to be more variable in

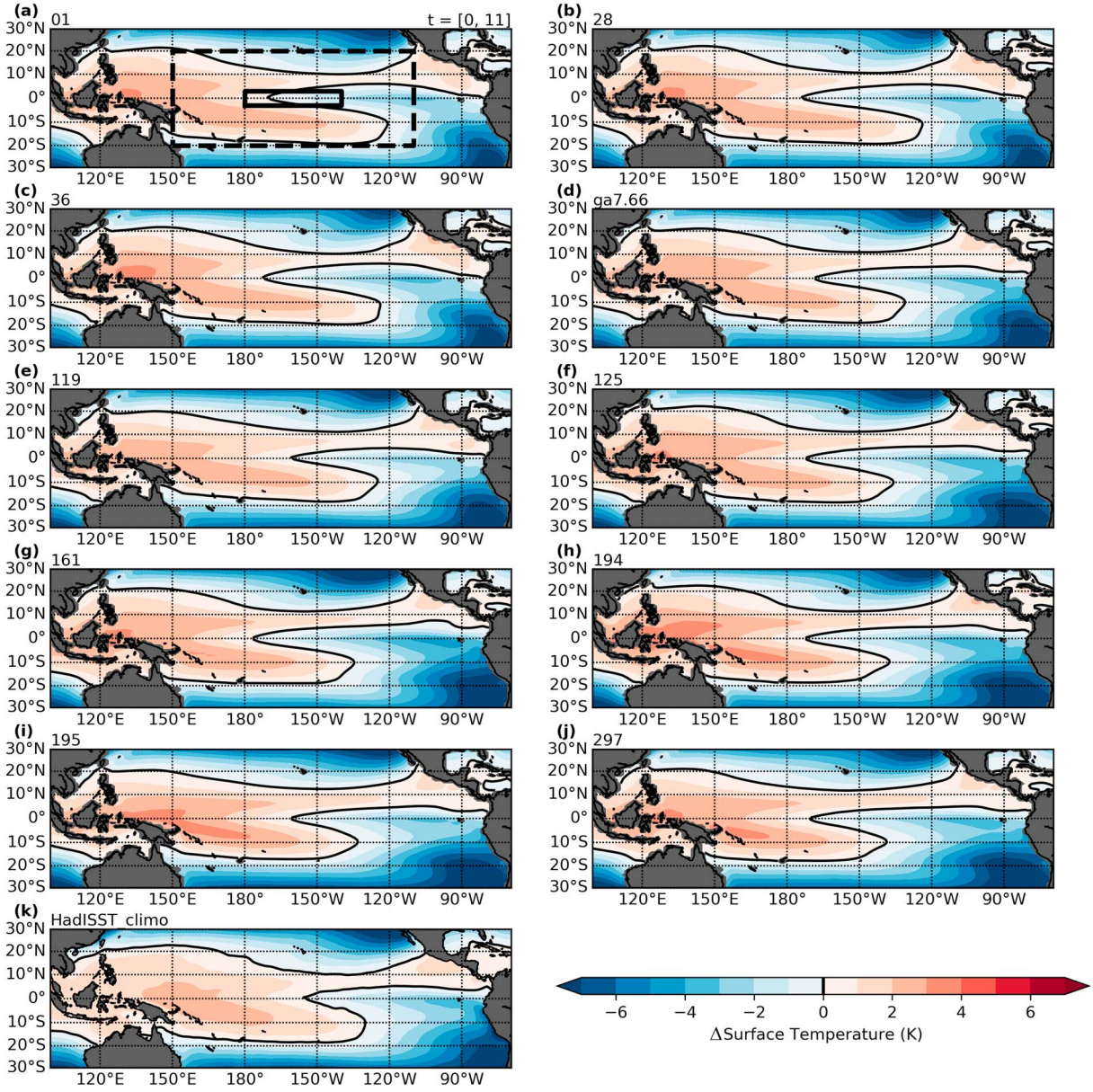

Figure 12. Annual mean SST as an anomaly from the tropical mean SST (−20°S to 20°N) for model versions (a) 01, (b) 28, (c) 36, (d) ga7.66, (e) 119, (f) 125, (g) 161, (h) 194, (i) 195, and (j) 297 and for (k) the HadISST climatology. The 0 K contour is plotted for reference in solid black. The cold tongue index is computed as the mean SST within the solid black box of (a) minus the mean SST within the black dashed box. SST = sea surface temperature.

ga7.66 and 119 than in other model versions (Figure 11). Further investigation of this variability is left as an avenue for future research. Figure 11 shows 20-year running means for 297 and GPCP as annual mean precipitation rates are available.

The averaging period examined for ga7.66 throughout most of this study, years 2–20, is a period of relatively weak double-ITCZ bias. -However, by the latest available climatology, the bias has grown to similar strength as the mean bias in 119, 2.0 mm/day. Similarly, the double-ITCZ bias in 119 is quite variable ranging from 1.5 mm/day for years 21–40 and 30–49 to 2.0 mm/day for years 2–21 and 75–99. By comparison, across the 300 years of output available for 297, no 20-year period has a double-ITCZ index above 1.7 mm/day, and the mean index value is below 1.5 mm/day, the minimum seen in both ga7.66 and 119. GPCP also shows weak variability, though the variability of the 20-year mean is constrained by the 30-year length of the observational record. Taken together, these results suggest that while model configurations ga7.66 and

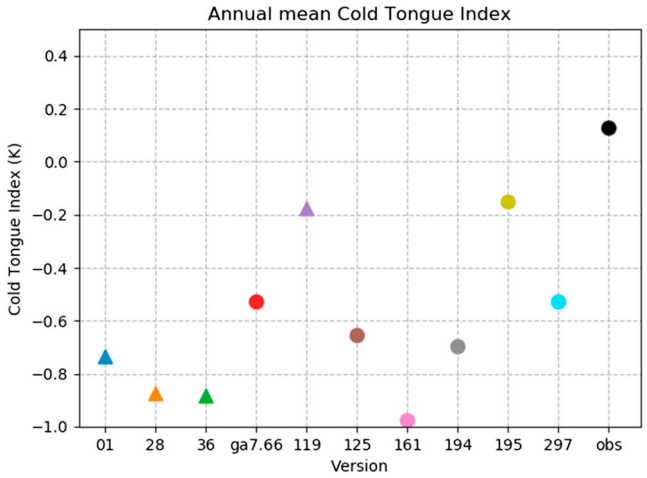

Figure 13. Annual mean cold tongue index as a function of model version. Model versions with an annual mean double-Intertropical Convergence Zone index greater than 2 mm/day are plotted with triangles. Model versions with a double-Intertropical Convergence Zone index below this threshold are plotted using circles.

119 are capable of simulating periods with a weak double-ITCZ bias, the SWCF bias present in the southeast Pacific of these models leads to a double-ITCZ bias in the long-term mean state.

3.4. The Cold Tongue Bias

Previous studies examining the role of southeast Pacific stratus and stratocumulus in setting the tropical Pacific SST and precipitation climatologies found increased southeast Pacific cloud cover weakened the double-ITCZ bias but amplified the cold tongue bias (Ma et al., 1996; de Szoeke et al., 2006; Yu & Mechoso, 1999). Given the improvements in the double-ITCZ bias in CESM2, one may expect a corresponding strengthening of the cold tongue bias. Figure 12 shows the annual mean tropical Pacific SST for each of the fully coupled simulations and the HadISST climatology as an anomaly from the corresponding tropical mean SST. In the HadISST climatology, the 0 K contour crosses the equator a few degrees east of 150°W. Model versions 119 and 195 are the closest to matching this equator crossing, but for most model versions, the equator crossing of the zero contour is displaced noticeably westward.

To quantitatively assess the cold tongue evolution across model versions, we use the cold tongue index from Woelfle et al. (2018): mean SST over the central Pacific cold tongue region (180° to 140°W; 3°S to 3°N; solid black box in Figure 12a) minus the mean SST averaged over the greater tropical Pacific basin (150°E to 110°W; 20°S to 20°N; dashed black box in Figure 12a). Using this metric, no trend appears in the annual mean cold tongue bias when examined as a function of model version (Figure 13). Restricting the averaging period to the months when the east Pacific ITCZ bias is at its maximum, February to May, yields similar results. Furthermore, the annual mean cold tongue bias across model versions exhibits no correlation with the double-ITCZ index of Bellucci et al., 2010 (2010; $r^2 = -0.01$). Because the cold tongue bias does not exhibit systematic improvement across model versions, we did not perform any further investigation into the evolution of this bias.

4. Conclusions and Summary

In this study, we examine a number of intermediate versions of CESM produced as part of the model development process for CESM2. We show that model versions 125 and later exhibit a robust improvement in simulating the east Pacific ITCZ. This increase is coincident with increased low cloud cover in the southeast Pacific stratocumulus to trade cumulus transition region. The increase in low cloud fraction increases the SWCF, shifting it toward more realistic values. This drives a corresponding decrease in net surface shortwave flux. The reduced surface shortwave heating leads to locally reduced SSTs in the southeast Pacific. In turn, this local SST change impacts the broader Pacific circulation by increasing the zonal pressure gradient associated with the Walker Circulation and by correcting the local springtime bias in the meridional pressure gradient. This process is similar to the results of Wang et al. (2015) who noted the east Pacific ITCZ pressure gradients are near zero in observations and therefore sensitive to small errors. Models with a poor representation of the east Pacific ITCZ have a southward springtime pressure gradient which drives anomalous cross equatorial flow into the southern hemisphere. Improved models have a springtime pressure gradient near zero. The dependency of the east Pacific ITCZ on the relative warmth of the southeast Pacific is consistent with the results shown in a broader study of the transition from CAM5 to CAM6 (Bogenschutz et al., 2018) and a previous study exploring the relationship between southeast Pacific SSTs and the double-ITCZ bias in CESM version 1 (Song & Zhang, 2016).

A series of simulations with prescribed SSTs shows the increase in low cloud cover between intermediate model version 119 and version 125 is attributable to changes in cloud microphysics rather than to retuning of the joint shallow convection-low cloud parameterization, CLUBB. In 119, the parameterized autoconversion and accretion rates include a dependence on cloud water variance. This dependency is removed in 125. Conceptually, including cloud water variance when computing these process rates is akin to assuming the cloud field is nonuniform with regions of heightened and depleted cloud water within the grid cell. Because autoconversion and accretion are nonlinear functions of cloud water content, the net process rates

are elevated under the assumption of heterogeneity. Thus, the removal of the cloud water variance dependency in 125 leads to a reduction in autoconversion and accretion rates and a corresponding decrease in the precipitation production in regions of large-scale warm rain. This allows the cloud fraction to remain elevated farther into the central Pacific as the cloud water sink due to drizzle is reduced. In turn, this results in increased SWCF over the southeast Pacific stratocumulus to trade cumulus transition region and improvement in the east Pacific ITCZ structure. The importance of the microphysical changes is further highlighted by the limited circulation response in the prescribed SST simulations.

Model version 119 also included a secondary cloud condensation scheme which was removed from 125 due to its being responsible for elevated cloud feedbacks in the coupled model. This so-called liquid supersaturation adjustment scheme acted on the model state following the call to cloud macrophysics. The scheme converted any water vapor above the level of saturation with respect to liquid water to liquid cloud droplets before the model state was passed to the cloud microphysics. Thus, removal of this scheme reduces the modeled condensation rate and yields similar impacts on southeast Pacific cloud cover and precipitation rates to the changes driven by the removal of cloud variance dependence in the autoconversion and accretion parameterizations. The removal of the liquid supersaturation scheme also led to increased precipitation in the northern branch of the ITCZ.

While the fixed-SST sensitivity simulations provided insight into the mechanisms leading to the increased cloud cover in 125 as compared to 119, the reasons for the increased cloud cover in CESM2 remain less well understood. The default autoconversion and accretion parameterizations in 119 and 125 are Seifert and Beheng (2001), while 297 uses Khairoutdinov and Kogan (2000). Furthermore, the autoconversion and accretion rates of 297 include the dependence on cloud water variance which was removed in 125. Thus, the increased cloud cover in the southeast Pacific in CESM2 is driven by different processes than the increase seen in 125. Regardless of the mechanism behind the increase in southeast Pacific cloud cover, the persistence of the increased cloud fraction from model version 125 onward is key to the local improvement in the double ITCZ of the east Pacific.

While the local improvements from 01 to 297 are dramatic, there is little systematic change in global, zonal mean ITCZ metrics or in the Pacific cold tongue bias. The SPCZ also remains too zonal, and precipitation rates in the northern branch of the east Pacific ITCZ are elevated when the southern hemisphere bias diminishes. The results shown in this study highlight the importance of local rather than remote processes for determining the structure of the east Pacific ITCZ and suggest further understanding of local processes in other tropical regions may be necessary to fully ameliorate the double-ITCZ and cold tongue biases in future fully coupled GCMs.

Acknowledgments
The work presented in this paper was funded by NSF AGS-1419507. Simulations presented in this study were performed on the National Center for Atmospheric Research's Yellowstone (http://n2t.net/ark:/85065/d7wd3xhc) and Cheyenne (Computational And Information Systems Laboratory, 2017) computing systems. Observational data and reanalysis output used in this study are available from the cited references. Model output used in this study is archived at Woelfle et al. (2019). Table S1 described the relationship between those files and the simulations presented in this paper. The authors would like to thank Andrew Gettelman for helpful discussions, Ilana Stern for her assistance in archiving the model output, and two anonymous reviewers for the their contributions toward improving this manuscript.

References

Bacmeister, J. T., Suarez, M. J., & Robertson, F. R. (2006). Rain reevaporation, boundary layer-convection interactions, and Pacific rainfall patterns in an AGCM. *Journal of the Atmospheric Sciences*, *63*(12), 3383–3403. https://doi.org/10.1175/JAS3791.1

Bellucci, A., Gualdi, S., & Navarra, A. (2010). The double-ITCZ syndrome in coupled general circulation models: The role of large-scale vertical circulation regimes. *Journal of Climate*, *23*(5), 1127–1145. https://doi.org/10.1175/2009JCLI3002.1

Bogenschutz, P. A., Gettelman, A., Hannay, C., Larson, V. E., Neale, R. B., Craig, C., & Chen, C. C. (2018). The path to CAM6: Coupled simulations with CAM5.4 and CAM5.5. *Geoscientific Model Development*, *11*(1), 235–255. https://doi.org/10.5194/gmd-11-235-2018

Broccoli, A. J., Dahl, K. A., & Stouffer, R. J. (2006). Response of the ITCZ to Northern Hemisphere cooling. *Geophysical Research Letters*, *33*, L01702. https://doi.org/10.1029/2005GL024546

Chiang, J. C. H., Biasutti, M., & Battisti, D. S. (2003). Sensitivity of the Atlantic Intertropical Convergence Zone to Last Glacial Maximum boundary conditions. *Paleoceanography*, *18*(4), 1094. https://doi.org/10.1029/2003PA000916

Chiang, J. C. H., & Bitz, C. M. (2005). Influence of high latitude ice cover on the marine Intertropical Convergence Zone. *Climate Dynamics*, *25*(5), 477–496. https://doi.org/10.1007/s00382-005-0040-5

Chiang, J. C. H., Cheng, W., & Bitz, C. M. (2008). Fast teleconnections to the tropical Atlantic sector from Atlantic thermohaline adjustment. *Geophysical Research Letters*, *35*, L07704. https://doi.org/10.1029/2008GL033292

Computational And Information Systems Laboratory (2017). Cheyenne: SGI ICE XA Cluster (University Community Computing). UCAR/NCAR, https://doi.org/10.5065/D6RX99HX

de Szoeke, S. P., Wang, Y., Xie, S. P., & Miyama, T. (2006). Effect of shallow cumulus convection on the eastern Pacific climate in a coupled model. *Geophysical Research Letters*, *33*, L17713. https://doi.org/10.1029/2006GL026715

Dee, D. P., Uppala, S. M., Simmons, A. J., Berrisford, P., Poli, P., Kobayashi, S., & Vitart, F. (2011). The ERA-Interim reanalysis: Configuration and performance of the data assimilation system. *Quarterly Journal of the Royal Meteorological Society*, *137*(656), 553–597. https://doi.org/10.1002/qj.828

DiNezio, P. N., Vecchi, G. A., & Clement, A. C. (2013). Detectability of changes in the Walker Circulation in response to global warming. *Journal of Climate*, *26*(12), 4038–4048. https://doi.org/10.1175/JCLI-D-12-00531.1

Dong, B. W., & Sutton, R. T. (2002). Adjustment of the coupled ocean-atmosphere system to a sudden change in the thermohaline circulation. *Geophysical Research Letters*, *29*(15), 1728. https://doi.org/10.1029/2002GL015229

Gettelman, A., & Morrison, H. (2014). Advanced two-moment bulk microphysics for global models. Part I: Off-line tests and comparison with other schemes. *Journal of Climate*, *28*(3), 1268–1287. https://doi.org/10.1175/JCLI-D-14-00102.1

Golaz, J. C., Larson, V. E., & Cotton, W. R. (2002a). A PDF-based model for boundary layer clouds. Part II: Model results. *Journal of the Atmospheric Sciences*, *59*(24), 3552–3571. https://doi.org/10.1175/1520-0469(2002)059<3552:APBMFB>2.0.CO;2

Golaz, J. C., Larson, V. E., & Cotton, W. R. (2002b). A PDF-based model for boundary layer clouds. Part I: Method and model description. *Journal of the Atmospheric Sciences*, *59*(24), 3540–3551. https://doi.org/10.1175/1520-0469(2002)059<3540:APBMFB>2.0.CO;2

Green, B., & Marshall, J. (2017). Coupling of trade winds with ocean circulation damps ITCZ shifts. *Journal of Climate*, *30*(12), 4395–4411. https://doi.org/10.1175/JCLI-D-16-0818.1

Guo, H., Golaz, J. C., Donner, L. J., Wyman, B., Zhao, M., & Ginoux, P. (2015). CLUBB as a unified cloud parameterization: Opportunities and challenges. *Geophysical Research Letters*, *42*, 4540–4547. https://doi.org/10.1002/2015GL063672

Hawcroft, M., Haywood, J. M., Collins, M., Jones, A., Jones, A. C., & Stephens, G. (2016). Southern Ocean albedo, inter-hemispheric energy transports and the double ITCZ: Global impacts of biases in a coupled model. *Climate Dynamics*, *48*, 2279–2295. https://doi.org/10.1007/s00382-016-3205-5

Hirota, N., Takayabu, Y. N., Watanabe, M., & Kimoto, M. (2011). Precipitation reproducibility over tropical oceans and its relationship to the double ITCZ problem in CMIP3 and MIROC5 climate models. *Journal of Climate*, *24*(18), 4859–4873. https://doi.org/10.1175/2011JCLI4156.1

Hubert, L. F., Krueger, A. F., & Winston, J. S. (1969). The double Intertropical Convergence Zone—Fact or fiction? *Journal of the Atmospheric Sciences*, *26*(4), 771–773. https://doi.org/10.1175/1520-0469(1969)026<0771:TDICZF>2.0.CO;2

Huffman, G. J., Adler, R. F., Bolvin, D. T., & Gu, G. (2009). Improving the global precipitation record: GPCP version 2.1. *Geophysical Research Letters*, *36*, L17808. https://doi.org/10.1029/2009GL040000

Hwang, Y. T., & Frierson, D. M. W. (2013). Link between the double-Intertropical Convergence Zone problem and cloud biases over the Southern Ocean. *Proceedings of the National Academy of Sciences*, *110*(13), 4935–4940. https://doi.org/10.1073/pnas.1213302110

Kang, S. M., Held, I. M., Frierson, D. M. W., & Zhao, M. (2008). The response of the ITCZ to extratropical thermal forcing: Idealized slab-ocean experiments with a GCM. *Journal of Climate*, *21*(14), 3521–3532. https://doi.org/10.1175/2007JCLI2146.1

Kang, S. M., Held, I. M., & Xie, S. P. (2014). Contrasting the tropical responses to zonally asymmetric extratropical and tropical thermal forcing. *Climate Dynamics*, *42*(7-8), 2033–2043. https://doi.org/10.1007/s00382-013-1863-0

Kang, S. M., Shin, Y., & Xie, S. P. (2018). Extratropical forcing and tropical rainfall distribution: Energetics framework and ocean Ekman advection. *npj Climate and Atmospheric Science*, *1*(1), 2. https://doi.org/10.1038/s41612-017-0004-6

Kay, J. E., Wall, C., Yettella, V., Medeiros, B., Hannay, C., Caldwell, P., & Bitz, C. (2016). Global climate impacts of fixing the Southern Ocean shortwave radiation bias in the Community Earth System Model (CESM). *Journal of Climate*, *29*, 4617–4636. https://doi.org/10.1175/JCLI-D-15-0358.1

Khairoutdinov, M., & Kogan, Y. (2000). A new cloud physics parameterization in a large-eddy simulation model of marine stratocumulus. *Monthly Weather Review*, *128*(1), 229–243. https://doi.org/10.1175/1520-0493(2000)128<0229:ANCPPI>2.0.CO;2

Li, G., & Xie, S. P. (2014). Tropical biases in CMIP5 multimodel ensemble: The excessive equatorial Pacific cold tongue and double ITCZ problems. *Journal of Climate*, *27*(4), 1765–1780. https://doi.org/10.1175/JCLI-D-13-00337.1

Lin, J. L. (2007). The double-ITCZ problem in IPCC AR4 coupled GCMs: Ocean-atmosphere feedback analysis. *Journal of Climate*, *20*(18), 4497–4525. https://doi.org/10.1175/JCLI4272.1

Lindzen, R. S., & Hou, A. V. (1988). Hadley circulations for zonally averaged heating centered off the equator. *Journal of the Atmospheric Sciences*, *45*(17), 2416–2427. https://doi.org/10.1175/1520-0469(1988)045<2416:HCFZAH>2.0.CO;2

Lindzen, R. S., & Nigam, S. (1987). On the role of sea surface temperature gradients in forcing low-level winds and convergence in the tropics. *Journal of the Atmospheric Sciences*, *44*(17), 2418–2436. https://doi.org/10.1175/1520-0469(1987)044<2418:OTROSS>2.0.CO;2

Liu, H., Zhang, M., & Lin, W. (2012). An investigation of the initial development of the double-ITCZ warm SST biases in the CCSM. *Journal of Climate*, *25*(1), 140–155. https://doi.org/10.1175/2011JCLI4001.1

Loeb, N. G., Wielicki, B. A., Doelling, D. R., Smith, G. L., Keyes, D. F., Kato, S., & Wong, T. (2009). Toward optimal closure of the Earth's top-of-atmosphere radiation budget. *Journal of Climate*, *22*(3), 748–766. https://doi.org/10.1175/2008JCLI2637.1

Ma, C. C., Mechoso, C. R., Robertson, A. W., & Arakawa, A. (1996). Peruvian stratus clouds and the tropical Pacific circulation: A coupled ocean-atmosphere GCM study. *Journal of Climate*, *9*(7), 1635–1645. https://doi.org/10.1175/1520-0442(1996)009<1635:PSCATT>2.0.CO;2

Mahajan, S., Saravanan, R., & Chang, P. (2011). The role of the wind-evaporation sea surface temperature (WES) feedback as a thermodynamic pathway for the equatorward propagation of high-latitude sea ice induced cold anomalies. *Journal of Climate*, *24*(5), 1350–1361. https://doi.org/10.1175/2010JCLI3455.1

Mechoso, C., Robertson, A., Barth, N., Davey, M., Delecluse, P., Gent, P., & Tribbia, J. (1995). The seasonal cycle over the tropical Pacific in coupled ocean-atmosphere general circulation models. *Monthly Weather Review*, *123*(9), 2825–2838. https://doi.org/10.1175/1520-0493(1995)123<2825:TSCOTT>2.0.CO;2

Mitchell, T. P., & Wallace, J. M. (1992). The annual cycle in equatorial convection and sea surface temperature. *Journal of Climate*, *5*(10), 1140–1156. https://doi.org/10.1175/1520-0442(1992)005<1140:TACIEC>2.0.CO;2

Neale, R. B., & Hoskins, B. J. (2000). A standard test for AGCMs including their physical parametrizations. II: Results for the Met Office Model. *Atmospheric Science Letters*, *1*(2), 108–114. https://doi.org/10.1006/asle.2000.0024

Oueslati, B., & Bellon, G. (2015). The double ITCZ bias in CMIP5 models: Interaction between SST, large-scale circulation and precipitation. *Climate Dynamics*, *44*(3-4), 585–607. https://doi.org/10.1007/s00382-015-2468-6

Rayner, N. A., Parker, D. E., Horton, E. B., Folland, C. K., Alexander, L. V., Rowell, D. P., & Kaplan, A. (2003). Global analyses of sea surface temperature, sea ice, and night marine air temperature since the late nineteenth century. *Journal of Geophysical Research*, *108*(D14), 4407. https://doi.org/10.1029/2002JD002670

Schneider, T. (2017). Feedback of atmosphere-ocean coupling on shifts of the Intertropical Convergence Zone. *Geophysical Research Letters*, *44*, 11644–11653. https://doi.org/10.1002/2017GL075817

Seifert, A., & Beheng, K. D. (2001). A double-moment parameterization for simulating autoconversion, accretion and selfcollection. *Atmospheric Research*, *59-60*, 265–281. https://doi.org/10.1016/S0169-8095(01)00126-0

Seo, J., Kang, S. M., & Frierson, D. M. W. (2014). Sensitivity of Intertropical Convergence Zone movement to the latitudinal position of thermal forcing. *Journal of Climate*, *27*(8), 3035–3042. https://doi.org/10.1175/JCLI-D-13-00691.1

Song, X., & Zhang, G. J. (2009). Convection parameterization, tropical Pacific double ITCZ, and upper-ocean biases in the NCAR CCSM3. Part I: Climatology and atmospheric feedback. *Journal of Climate*, *22*(16), 4299–4315. https://doi.org/10.1175/2009JCLI2642.1

Song, F., & Zhang, G. J. (2016). Effects of southeastern Pacific sea surface temperature on the double-ITCZ bias in NCAR CESM1. *Journal of Climate*, *29*, 7417–7433. https://doi.org/10.1175/JCLI-D-15-0852.1

Sun, Q., Whitney, M. M., Bryan, F. O., & Tseng, Y. H. (2017). A box model for representing estuarine physical processes in Earth system models. *Ocean Modelling*, *112*, 139–153. https://doi.org/10.1016/j.ocemod.2017.03.004

Taylor, K. E., Stouffer, R. J., & Meehl, G. A. (2012). An overview of CMIP5 and the experiment design. *Bulletin of the American Meteorological Society*, *93*(4), 485–498. https://doi.org/10.1175/BAMS-D-11-00094.1

Tomas, R. A., Deser, C., & Sun, L. (2016). The role of ocean heat transport in the global climate response to projected Arctic sea ice loss. *Journal of Climate*, *29*(19), 6841–6859. https://doi.org/10.1175/JCLI-D-15-0651.1

Waliser, D. E., & Gautier, C. (1993). A satellite-derived climatology of the ITCZ. *Journal of Climate*, *6*(11), 2162–2174. https://doi.org/10.1175/1520-0442(1993)006<2162:ASDCOT>2.0.CO;2

Wang, C. C., Lee, W. L., Chen, Y. L., & Hsu, H. H. (2015). Processes leading to double Intertropical Convergence Zone bias in CESM1/CAM5. *Journal of Climate*, *28*, 2900–2915. https://doi.org/10.1175/JCLI-D-14-00622.1

Woelfle, M. D., Bretherton, C. S., Hannay, C., & Neale, R. (2019). Woelfle et al. (2019) data [Data set], UCAR/NCAR - Earth System Grid, https://doi.org/10.5065/73AM-EH65

Woelfle, M. D., Yu, S., Bretherton, C. S., & Pritchard, M. S. (2018). Sensitivity of coupled tropical Pacific model biases to convective parameterization in CESM1. *Journal of Advances in Modeling Earth Systems*, *10*, 126–144. https://doi.org/10.1002/2017MS001176

Yoshimori, M., & Broccoli, A. J. (2008). Equilibrium response of an atmosphere-mixed layer ocean model to different radiative forcing agents: Global and zonal mean response. *Journal of Climate*, *21*(17), 4399–4423. https://doi.org/10.1175/2008JCLI2172.1

Yoshimori, M., & Broccoli, A. J. (2009). On the link between Hadley circulation changes and radiative feedback processes. *Geophysical Research Letters*, *36*, L20703. https://doi.org/10.1029/2009GL040488

Yu, J. Y., & Mechoso, C. R. (1999). Links between annual variations of Peruvian stratocumulus clouds and of SST in the eastern equatorial Pacific. *Journal of Climate*, *12*(11), 3305–3318. https://doi.org/10.1175/1520-0442(1999)012<3305:LBAVOP>2.0.CO;2

Zhang, C. (2001). Double ITCZs. *Journal of Geophysical Research*, *106*(D11), 11,785–11,792. https://doi.org/10.1029/2001JD900046

Zhang, X., Lin, W., & Zhang, M. (2007). Toward understanding the double Intertropical Convergence Zone pathology in coupled ocean-atmosphere general circulation models. *Journal of Geophysical Research*, *112*, D12102. https://doi.org/10.1029/2006JD007878